

Unbounded Orbits for Outer Billiards

Richard Evan Schwartz *

May 16, 2019

Abstract

The question of B.H. Neumann, which dates back to the 1950s, asks if there exists an outer billiards system with an unbounded orbit. We prove that outer billiards for the Penrose kite, the convex quadrilateral from the Penrose tiling, has an unbounded orbit. We also analyze some finer properties of the orbit structure, and in particular produce an uncountable family of unbounded orbits. Our methods relate outer billiards on the Penrose kite to polygon exchange maps, arithmetic dynamics, and self-similar tilings.

1 Introduction

1.1 History of the Problem

Outer billiards is a basic dynamical system which serves as a toy model for celestial mechanics. See Sergei Tabachnikov's book [T], and also the survey [DT], for an exposition of the subject and many references.

To define an outer billiards system, one starts with a bounded convex set $S \subset \mathbf{R}^2$ and considers a point $x_0 \in \mathbf{R}^2 - S$. One defines x_1 to be the point such that the segment $\overline{x_0x_1}$ is tangent to S at its midpoint and S lies to the right of the ray $\overrightarrow{x_0x_1}$. (See Figure 1.1 below.) The point x_1 is not well-defined if $\overline{x_0x_1}$ is tangent to S along a segment. This will inevitably happen sometimes when S is a polygon. Nonetheless, the outer billiards construction is almost everywhere well defined. The iteration $x_0 \rightarrow x_1 \rightarrow x_2 \dots$ is called the *outer billiards orbit* of x_0 .

* This research is supported by N.S.F. Grant DMS-0305047

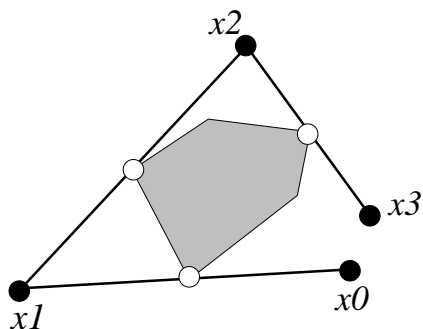


Figure 1.1: Outer Billiards

B.H. Neumann ¹ introduced outer billiards during some lectures for popular audiences given in the 1950s. See, e.g. [N]. J. Moser popularized the construction in the 1970s. Moser [M, p. 11] attributes the following question to Neumann *circa* 1960, though it is sometimes called *the Moser Conjecture*.

Question: *Is there an outer billiards system with an unbounded orbit?*

There have been several results related to this question.

- Moser [M] sketches a proof, inspired by K.A.M. theory, that outer billiards on S has all bounded orbits provided that ∂S is at least C^6 smooth. (R. Douady [D] gives a complete proof in his thesis, some of which is still unpublished.)
- In [VS], [Ko], and (later, but with different methods) [GS], it is proved that outer billiards on a *quasirational polygon* has all orbits bounded. This class of polygons includes polygons with rational vertices and also regular polygons. In the rational case, all defined orbits are periodic.
- Tabachnikov analyzes the outer billiards system for the regular pentagon and shows that there are some infinite (but bounded) orbits. See [T, p 158] and the references there.
- Genin [G] shows that all orbits are bounded for the outer billiards systems associated to trapezoids. He also makes a brief numerical study of a particular irrational kite based on the square root of 2, observes possibly unbounded orbits, and indeed conjectures that this is the case.

¹My information on this comes from 1999 email correspondence between Bernhard Neumann and Keith Burns, and also from Bernhard's son Walter.

1.2 The Main Result

The main goal of this paper is to prove:

Theorem 1.1 *Outer billiards on the Penrose kite has an unbounded orbit. In fact, both the forwards and backwards orbits of the point p shown in Figure 1.2 are entirely defined and unbounded.*

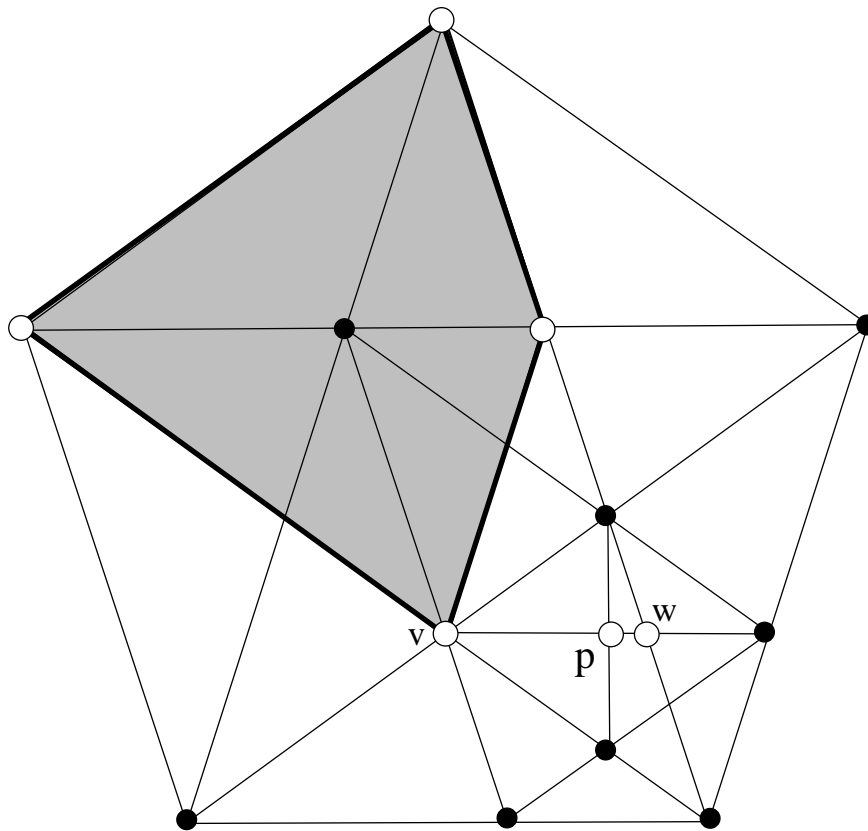


Figure 1.2: The Penrose Kite

The *Penrose kite* is the convex quadrilateral that appears in the Penrose tiling. Figure 1.2 below shows a classic construction of the Penrose kite—the shaded figure—based on a regular pentagon. The additional lines show how the point p is constructed. The significance of the points v and w will be explained in Theorem 1.2 below.

1.3 Outline of the Proof

We will give a rigorous computer-assisted proof of Theorem 1.1. We think that our proof gets close to the conceptual core of what is going on, but we need a lot of computation to make it go. Here are the main ideas.

- Replacing the Penrose kite by the affinely equivalent image S , we arrive at an outer billiards system that is defined over the ring $\mathbf{Z}[\phi]$, where ϕ is the golden ratio. (Outer billiards is an affinely natural system.) Thus the outer billiards system respects subsets of the form \mathcal{C}^2 , where $\mathcal{C} \subset \mathbf{Q}[\phi]$ is any $\mathbf{Z}[\phi]$ -module. We make a particular choice of \mathcal{C} and treat it as a rank two \mathbf{Z} -module. In this way, we get an induced dynamical system on a subset of \mathbf{Z}^4 .
- There is a union $H \subset \mathbf{Z}^4$ consisting roughly of the intersection of \mathbf{Z}^4 with two 2-dimensional parallel halfplanes. When we encode the structure of the return map $\Upsilon_R : H \rightarrow H$ we arrive at an infinite polygonal subset $\Gamma \subset \mathbf{R}^2$, with the vertices in \mathbf{Z}^2 . We call Γ the *arithmetic graph*. (See Figures 2.3.1 and 2.3.2.)
- The structure of Γ is controlled by a polygon exchange map defined on the square torus T^2 . This 2-dimensional polygon exchange map arises as a certain slice of a piecewise affine map of the 4-torus we produce by re-topologizing $\mathbf{R}^2 - S$ in a way that is compatible with Υ_R and then compactifying. We have completely explicit formulas for this unlikely construction.
- Our 2-dimensional polygon exchange map is compatible with a kind of multi-valued contraction of T^2 . The graph of this correspondence is an irrationally embedded complex line sitting inside $T^2 \times T^2$. Rick Kenyon tells me that this picture is essentially the same as what one sees in the *cut and project* method from the theory of quasi-crystals.
- The interaction between the polygon exchange map and the multi-valued contraction forces Γ to behave like an aperiodic tiling with an inflation rule. When we dilate Γ about the origin by ϕ^3 we find that the dilated image is very closely shadowed by the original image. This structure forces the connected component Γ_0 of Γ containing the origin to be unbounded and this translates into the unboundedness of the orbit of the point p shown in Figure 1.2.

1.4 Orbit Structure

Our proof of Theorem 1.1 gives us information about the fine orbit structure of outer billiards on the Penrose kite. To make our result below more concise we will only consider the even iterates of points under the outer billiards map. However, we will implicitly mean that the odd iterates are also defined.

First, we will see easily that the distance from the n th point in $O_+(p)$, the forwards orbit of p , to the origin is a proper function of n . (A function $f : \mathbf{N} \rightarrow \mathbf{N}$ is *proper* if $f^{-1}[1, n]$ is bounded for all $n \in \mathbf{N}$.) In contrast, the backwards orbit $O_-(p)$ returns densely to a certain Cantor set.

Given a horizontal interval $I \subset \mathbf{R}^2$ and some $\lambda \in (0, 1)$ let $C(I, \lambda) \subset I$ denote the limit set of the semigroup generated by the two contractions of strength λ that map I into itself and fix an endpoint of I . Note that $C(I, \lambda)$ is a Cantor set.

Let γ_0 be the similarity of strength $-\lambda$ (orientation reversing) that maps $C(I, \lambda)$ to the right half of $C(I, \lambda)$. Likewise, we define γ_1 to be the similarity of strength $-\lambda$ that maps $C(I, \lambda)$ to the left half of $C(I, \lambda)$. There is a unique homeomorphism $\theta_2 : \mathbf{Z}_2 \rightarrow C$ that conjugates γ_j to the map $x \rightarrow 2x + j$. We call θ_2 the *twist homeomorphism* because (in our imagination) it has the effect of twisting at every scale. θ_2 maps the points of $\mathbf{Z} - \frac{1}{3}\mathbf{Z}$ to the *gap points* of C , those points which are endpoints of the components of $I - C$. In particular $\theta_2(-1/3)$ and $\theta_2(-2/3)$ are the left and right endpoints of C .

Theorem 1.2 *Let $C = C([v, w], \phi^{-3})$, where v and w are as in Figure 1.2 and ϕ is the golden ratio. Let C^* denote C minus its gap points. The forwards and backwards orbits of every point of C^* are defined and unbounded. Moreover:*

- $O_-(p)$ returns to C densely, and $\theta_2(n)$ is the n th point of $O_-(p) \cap C$. In particular $\theta_2(0) = p$. Here θ_2 is the twist homomorphism.
- The forwards orbit of every point $x \in C^* - \{\theta_2(0)\}$ returns to C^* as the point x_- , where $\theta_2^{-1}(x_-) = \theta_2^{-1}(x) - 1$. The return time and excursion distance are both proper functions of the $1/\|x - \theta_2(0)\|$.
- The backwards orbit of every point $x \in C^* - \{\theta_2(-1)\}$ returns to C^* as the point x_+ , where $\theta_2^{-1}(x_+) = \theta_2^{-1}(x) + 1$. The return times and excursion distances are both proper functions of $1/\|x - \theta_2(-1)\|$.

In the third item, the *return time* denotes the number of iterates of $O_+(x)$ between x and x_- . The *excursion distance* denotes the maximum norm of such an iterate. The terms in the fourth item have similar meanings.

C^* serves as a kind of section for (some of) outer billiards on the Penrose kite. The return map to C^* , defined except at 2 points, is conjugate to the so-called *2-adic adding machine*, and the return times and excursion distances are proper functions of the inverse 2-adic distances to the two special points.

Theorem 1.2 implies that there are uncountably many unbounded orbits of the outer billiards map on the Penrose kite with the following wild behavior: If V is any neighborhood of the vertex v and U is any neighborhood of ∞ , then both the forwards and backwards orbits oscillate between U and V infinitely often.

1.5 Discussion

Here are some remarks on the origins of Theorem 1.1. Let S' be the Penrose kite. It appears that $\mathbf{R}^2 - S' = A \cup B \cup C$ where

- A is a dynamically invariant union of finite sided polygons. All the orbits in a polygon have the same combinatorial type.
- B is a countable union of line segments consisting of the points on which the outer billiard map is undefined. B is the so-called *discontinuity set*.
- C is a fractal set consisting entirely of unbounded orbits.

Tabachnikov develops a similar picture for the the regular pentagon and the regular 7-gon, except that his region C consists of aperiodic but bounded orbits. Indeed, the picture for the 7-gon is shown on the cover of his book [T]. Inspired by the picture on the cover of Tabachnikov's book, I designed a computer program, *Billiard King* ² so that the user can draw this partition for an essentially arbitrary quadrilateral.

When the quadrilateral has rational vertices, C is empty and A is a locally finite tiling. I searched ³ through the parameter space of rational quadrilaterals for examples where A featured small tiles having widely ranging orbits.

²One can download this Java program from my website: www.math.brown.edu/~res

³Had I known earlier about Genin's numerical study, mentioned above, I perhaps would have saved time.

Eventually I considered kites having vertices with Fibonacci number coordinates, and this led to the Penrose kite.

I hope to find purely conceptual proofs for the results in this paper, but my first goal is just to establish them as true statements. Many people do not like computer-aided proofs, so I would like to say several things in favor of the proof I have given. First of all, it is the best I could do and there are no other proofs for results like these. Second, the proof is not *just* a calculation—there are plenty of concepts in it. Finally, I was able to check essentially all the details in the proof using Billiard King, so this proof has a lot of computational safeguards that one might not see in a traditional proof.

I tried as hard as possible to write a proof that is independent from Billiard King, but still the reader of this paper would get a much greater appreciation for what is going on by learning to use Billiard King. A few minutes playing with Billiard King is worth hours of reading the paper.

In a sequel paper I plan to revisit this subject and explore it more deeply. One might wonder if there is a natural level of generality for the above kinds of results and phenomena. For instance, ongoing experimentation with Billiard King suggests strongly that similar things happen for quadratically irrational kites in general. I plan to study this next.

1.6 Organization of the Paper

Our paper divides into three parts. In §2-5 we prove Theorems 1.1 and 1.2 modulo a technical result, the Arithmetic Graph Lemma. In §6 we prove the Arithmetic Graph Lemma. In §7-8 we describe our calculations in enough detail so that the interested reader could reproduce them. Here is a more detailed overview of the paper.

Part 1: In §2 we will reduce Theorem 1.1 to the statement that Γ_0 admits what we call an *inflation structure*. Essentially this means that certain smallish subsets (which we call *genes*) of Γ_0 are, when dilated by ϕ^3 , closely shadowed by other subsets of Γ_0 . In §3 we look more deeply at the interaction between the arithmetic graph and the polygon exchange map, reducing the existence of an inflation structure to something we call an *inflation generator*. We will be able to verify the existence of an inflation generator from a finite amount of computation. In §4 we explain how we actually check, with a finite amount of integer arithmetic computations, that there really exists an inflation generator for Γ_0 . The key point is that everything in sight

is defined over $\frac{1}{2}\mathbf{Z}[\phi]$. in §5 we prove Theorem 1.2 by taking a close look at the specifics of our inflation generator.

Part 2: In §6 we factor the return map for outer billiards into the product of 8 simpler maps, which we call *strip maps*. (Actually, the decomposition involves a fairly trivial 9th map as well. Equation 29 for a precise equation.) We then show how each strip map actually is compatible with a certain compactification of $\mathbf{R}^2 - S$: The space $\mathbf{R}^2 - S$ embeds densely as a locally planar set in the 4-torus, and each strip map extends to act as a piecewise affine transformation of the 4-torus. The composition of the extensions preserves a certain union of two 2-tori, and acts there as a polygon exchange. The Arithmetic Graph Lemma is a fairly direct consequence of this structure.

Part 3: In §7 we describe pseudo-code versions of the code we use to make our computations. In §8 we include the data used in our calculations. All the calculations described in §7-8 are implemented in Billiard King. Billiard King is a massive program, but we have placed all the computations relevant to the actual proof into separate files, so that they are easier to survey. We have tried to document Billiard King to the extent that the interested reader can survey the code and also re-run our computations.

1.7 Acknowledgements

I would like to thank Jeff Brock, Keith Burns, Peter Doyle, David Dumas, Eugene Gutkin, Pat Hooper, Richard Kent, Rick Kenyon, and Curt McMullen for helpful and interesting discussions related to this work. I would especially like to thank Sergei Tabachnikov for his technical and historical input and encouragement.

2 The Proof in Broad Strokes

2.1 An Affinely Equivalent Shape

The Penrose kite is affinely equivalent to the quadrilateral with coordinates

$$(0, 1); \quad (-1, 0); \quad (0, -1); \quad (A, 0); \quad A = \phi^{-3} \quad (1)$$

where ϕ is the golden ratio. The affine equivalence maps the point p in Figure 1.2 to the point

$$(\phi^{-2}, -1). \quad (2)$$

To clarify the logic of our argument, it is useful to consider a general value of $A \in (0, 1)$ for the moment. We define $T : \mathbf{Z}^2 \rightarrow \mathbf{R}^2$ via the formula

$$T(x, y) = 2Ax + 2y + \frac{1 - A}{2}. \quad (3)$$

The point in Equation 2 is $(T(0, 0), 1)$ when $A = \phi^{-3}$.

Lemma 2.1 *The outer billiards map is entirely defined on any point of the form*

$$T(\mathbf{Z}^2) \times \{\pm 1\}$$

In particular, the entire orbit of the point in Equation 2 is defined.

Proof: Let L denote the family of horizontal lines in \mathbf{R}^2 whose y -coordinates are odd integers. The outer billiards map preserves L . The only points where the the first iterate of the outer billiards map is undefined are points of the form $l \cap e$, where l is a line of L and e is a line extending an edge of the Penrose kite. One can check easily, given Equation 1.1, that all such points have first coordinates of the form $m + An$, where $m, n \in \mathbf{Z}$. On the other hand, no point of $T(\mathbf{Z}^2) \times \{\pm 1\}$ has this form, and no iterate of such a point has this form. ♠

Let Υ denote the square of the outer billiards map. Let $\mathcal{C} = T(\mathbf{Z}^2) \times \mathbf{Z}'$, where \mathbf{Z}' is the set of odd integers. The vector $\Upsilon(x) - x$ is always twice the difference between two of the vertices of our shape S . Given Equation 1.1, we see that the first coordinate of $\Upsilon(x) - x$ always has the form $2m + 2nA$ where m and n are integers. The second coordinate is always an even integer. Hence Υ is entirely defined on \mathcal{C} and preserves this set.

2.2 The Arithmetic Graph

Let

$$\mathcal{C}(\pm) = (T(\mathbf{Z}^2) \cap \mathbf{R}^+) \times \{\pm 1\}, \quad (4)$$

where T is as in Equation 3, and $A = \phi^{-3}$. (Henceforth we take $A = \phi^{-3}$.) The set $\mathcal{C}(\pm)$ is dense in the union of two rays starting at $(0, \pm 1)$ and parallel to $(1, 0)$. The point in Equation 2 belongs to $\mathcal{C}(\pm)$.



Figure 2.1: The objects S and $\mathcal{C}(\pm)$.

Υ does not preserve $\mathcal{C}(\pm)$, but we have ⁴ the first return map:

$$\Upsilon_R : \mathcal{C}(\pm) \rightarrow \mathcal{C}(\pm). \quad (5)$$

Our idea is to encode the structure of Υ_R graphically. We join $x_1, x_2 \in \mathbf{Z}^2$ by a segment iff $T(x_j) > 0$ for $j = 1, 2$, and there are choices $\epsilon_1, \epsilon_2 \in \{-1, 1\}$ such that

$$\Upsilon_R(T(x_1), \epsilon_1) = (T(x_2), \epsilon_2). \quad (6)$$

We let $\Gamma \subset \mathbf{R}^2$ be the resulting graph. We call Γ the *arithmetic graph*.

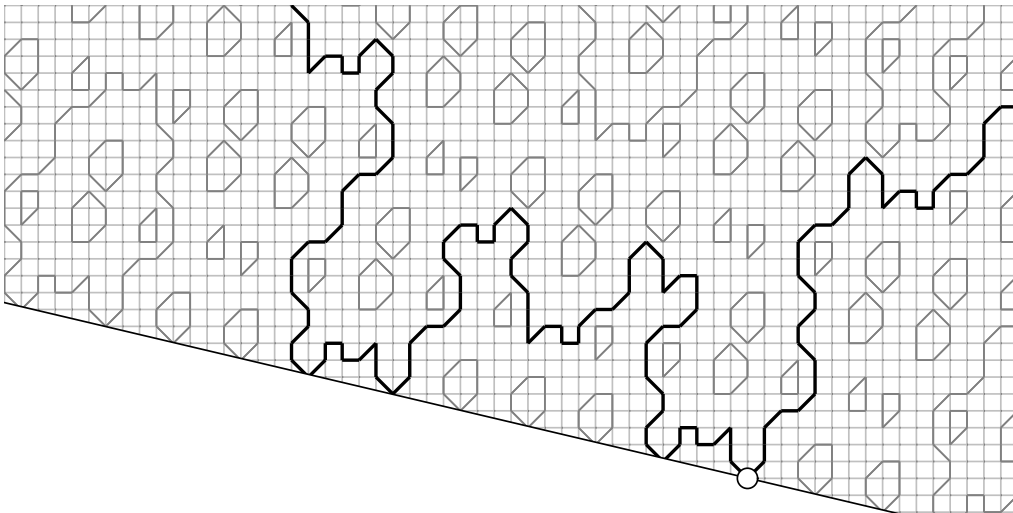


Figure 2.2: Part of the arithmetic graph

⁴A “runway” like the one in Figure 2.1, as well as a map somewhat like Υ_R , is also considered in [GS].

Figure 2.2 shows a small portion of Γ . The dot is $(0, 0)$. The component Γ_0 containing $(0, 0)$ is drawn in black. The grid indicates \mathbf{Z}^2 .

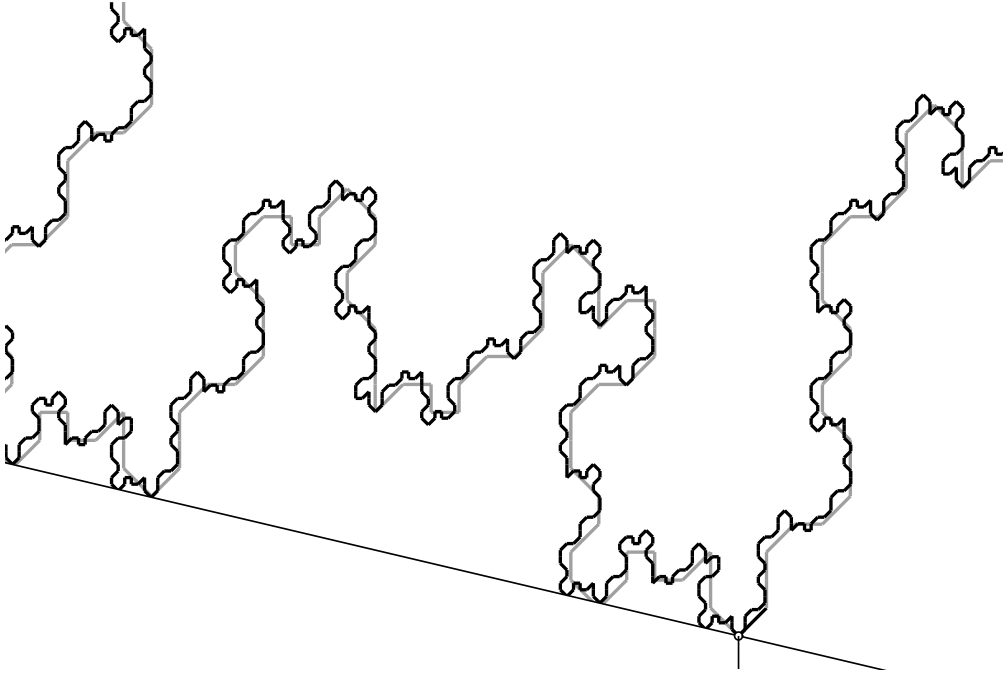


Figure 2.3: More of the component Γ_0 .

Figure 2.3 shows more of Γ_0 , again drawn in black. The origin is denoted by a little vertical line segment touching ∂H at its top endpoint. We have erased the other components and deleted the grid, to get a clearer picture. (The reader should use Billiard King to see really great pictures of Γ .) The curve Γ_0 , and indeed all of Γ , behaves like the self-similar inflationary tilings studied in [Ke]. One might call Γ a “large-scale fractal”.

Here is what we mean by *inflationary*: In Figure 2.3, there is also a grey curve running alongside Γ_0 . This grey curve is the dilated image $\phi^3\Gamma_0$. In other words, we dilate Γ_0 by ϕ^3 (about the origin), color it grey, and superimpose it on the original picture. From what we can see of the picture, it looks like Γ_0 and $\phi^3\Gamma_0$ closely follow each other. One might say that Γ_0 is *quasi-invariant* under a dilation. If this is true—and we will prove it below—then both ends of Γ_0 must exit every tubular neighborhood of ∂H . (Below we formulate this principle precisely.) Theorem 1.1 follows immediately from the fact that both ends of Γ_0 exit every tubular neighborhood of ∂H .

2.3 The Arithmetic Graph Lemma

Let $\mathbf{T}^2 = (\mathbf{R}/\mathbf{Z})^2$ be the square torus. Given $p \in \mathbf{R}^2$ let $[p]$ denote the projection to \mathbf{T}^2 . We define $\Psi : \mathbf{Z}^2 \rightarrow \mathbf{T}^2$ with the equation

$$\Psi(x, y) = \left[\left(\frac{T(x, y)}{2\phi}, \frac{T(x, y)}{2} \right) \right] = \left[\left(\phi^{-4}x + \phi^{-1}y, \phi^{-3}x \right) + \frac{1}{2}(\phi^{-3}, \phi^{-2}) \right]. \quad (7)$$

Here T is the map from Equation 3. The second equation is a direct calculation, which we omit. Clearly $T(\mathbf{Z}^2)$ is dense in \mathbf{T}^2 .

Given $v \in \mathbf{Z}^2 \cap H$ we define the *local type* of v to be the isometry type of the edges of Γ emanating from v . It turns out that there are 15 types (including the type where no edges emanate from v) but we prefer to label these 15 types by the integers $1, \dots, 26$ according to Figure 2.4. Most of these types can be seen in Figure 2.3. Notice that the picture for the even type $2k$ is obtained by rotating the picture for the odd type $2k - 1$ by 180 degrees.

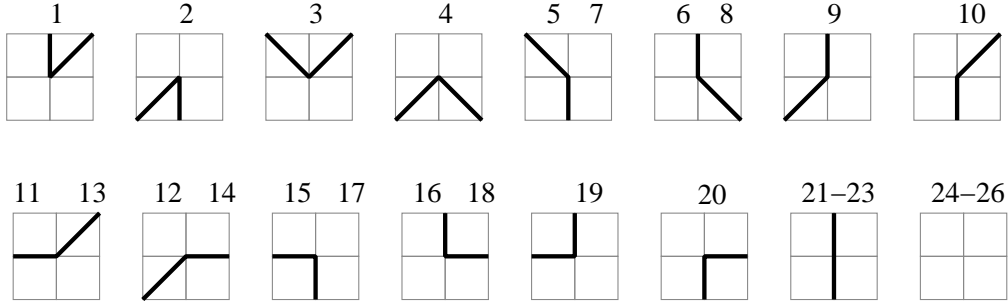


Figure 2.4: The local types

Figure 2.5 shows a partition of \mathbf{T}^2 into 26 open convex polygons P_1, \dots, P_{26} .

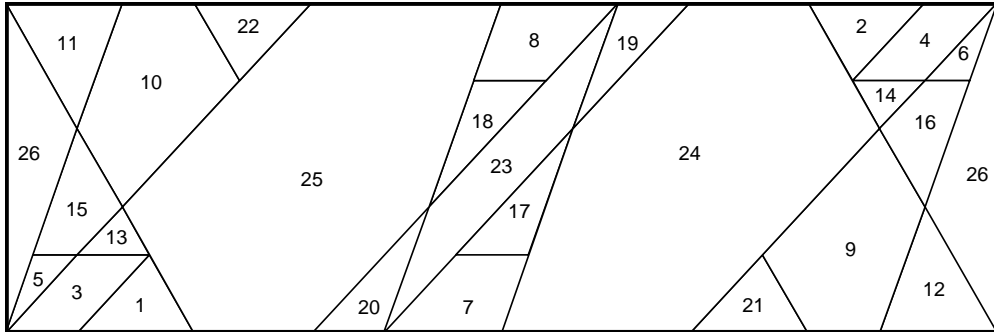


Figure 2.5: The Torus Partition

We have changed the aspect ratio so as to get a nicer picture. The true geometric picture is contained in the unit square, with sides identified as usual. The origin $(0,0)$ is the bottom left corner. The only polygon that “wraps” around is P_{26} . In §6 we will prove

Lemma 2.2 (Arithmetic Graph) Ψ maps each $x \in \mathbf{Z}^2 \cap H$ into some polygon of \mathcal{P} , and x has local type k if and only if $\Psi(x) \in P_k$.

The next result is not needed for our results, but it is nice to know and it illustrates the power of the Arithmetic Graph Lemma.

Lemma 2.3 *The arithmetic graph is an embedded union of polygons and polygonal arcs.*

Proof: (Sketch.) If some arc of the arithmetic graph crossed some other arc then would have a point (x, y) of type a and a point $(x + 1, y)$ of type b , where $a \in \{4, 6, 8\}$ and $b \in \{2, 4, 9, 12, 14\}$. But $v = \Psi(x + 1, y) - \Psi(x, y)$ is the vector (ϕ^{-3}, ϕ^{-4}) . This vector is the one that points from the lower left corner of P_3 to the upper right corner of P_3 in Figure 2.5, when it is anchored at the point $(0, 0)$. Looking carefully at Figure 2.5 we see that no position of v has this property. ♠

2.4 Inflation Structures

As we mentioned above, the basic idea in our proof that Γ_0 rises unboundedly far away from ∂H is to show that Γ_0 is quasi-invariant under the dilation

$$D(x, y) = (\phi^3 x, \phi^3 y). \tag{8}$$

In this section we formalize this idea.

Say that a *gene* is a (combinatorial) length 6 connected component of Γ_0 . Each gene has 5 interior vertices lying in \mathbf{Z}^2 . It turns out that there are 75 genes up to translation equivalence. That is, there are 75 combinatorial types of gene. Each gene A has a *core* B , consisting of the central path of length 2. Figure 2.6 shows two consecutive genes, and their cores. We say that $p' \in \mathbf{Z}^2$ *shadows* such a point $p \in \mathbf{R}^2$ if $\|p - p'\| < 4$. (Here 4 is a convenient cutoff.) Let B be a gene core, as above. We say that a finite polygonal path $A' \subset \Gamma$ *shadows* $D(B)$ if each endpoint of A' shadows a corresponding endpoint of $D(B)$. Figure 2.6 shows a combinatorially accurate example.

contains $(0, 0)$. Then $\chi(A_0)$ contains $(0, 0)$ and the consecutive paths $\chi(A_0)$, $\chi(A_1)$, $\chi(A_2), \dots$ fit together. These paths therefore trace out Γ_1 and rise up at least (say) $\phi^3(d - 10) - 10$, a quantity which is at least $2d$. Thus we see that Γ_1 actually rises up $2d$ units from ∂H . Iterating, we get our result. ♠

Remark:

Our argument above immediately proves that the distance from the origin to the n th point in $O_+(p)$ is a proper function of n .

3 Manufacturing an Inflation Structure

3.1 Dynamical Polygons

In this chapter we delve more deeply into the connection between the arithmetic graph Γ and the torus partition \mathcal{P} . We assume the truth of the Arithmetic Graph Lemma, which we prove in §6-8. In this chapter, we will not explicitly talk about polygon exchange maps, but the reader familiar with these objects will probably see the underlying connection.

Say that a *pointed strand* of Γ is a pair (X, x) , where X is a finite polygonal arc of Γ having length at least 2, and x is a vertex of X . Say that two pointed (X_1, x_1) and (X_2, x_2) strands are *equivalent* if there is a translation of \mathbf{Z}^2 carrying one to the other. We also require that $\Psi(x_1)$ and $\Psi(x_2)$ belong to the same polygon P_j of \mathcal{P} . Say that a *pointed strand type* is an equivalence class of pointed strands. Given a pointed strand type $\sigma = [(X, x)]$, we say that the *length* of σ is the length of X .

Here is an example. if we consider pairs (X, x) , where X has length 2 and x is the center vertex, then Figure 2.4 shows the 23 different equivalence classes. We call these equivalence classes the *local types*, as in §2.

For any pointed strand type σ let P_σ denote the closure of the set

$$\bigcup_x \Psi(x).$$

The union is taken over all vertices x such that $\sigma = [(X, x)]$ for some arc X . For instance, if σ is the j th of the 23 equivalence classes just discussed, then $P_\sigma = P_j$, the j th convex polygon in the partition \mathcal{P} . In general, we call P_σ a *dynamical polygon*. We give P_σ this name because it is generated by a dynamical process associated to the partition \mathcal{P} .

Lemma 3.1 (Dynamical Polygon) *Let σ be any pointed strand. Then P_σ is a convex polygon. Moreover, given $a \in \mathbf{Z}^2$, we have $a \in P_\sigma$ if and only if there is some arc $A \subset \Gamma$ such that $\sigma = [(A, a)]$.*

Proof: This is a proof by induction on the length of σ . We have already seen that our result is true when σ is a local type, as discussed above. Before we start our induction proof we observe a certain symmetry of our definition. Suppose that $\sigma_1 = [(X, x_1)]$ and $\sigma_2 = [(X, x_2)]$, where x_1 and x_2 are adjacent vertices of X . In general, we have

$$x_2 = x_1 + (\epsilon_1, \epsilon_2); \quad \epsilon_j \in \{-1, 0, 1\}. \quad (9)$$

Equation 7 gives us

$$\Psi(x_2) = \Psi(x_1) + (\epsilon_1\phi^{-4} + \epsilon_2\phi^{-1}, \epsilon_1\phi^{-3}).$$

This equation makes sense because T^2 is canonically an abelian group. Hence P_{σ_1} and P_{σ_2} are isometric to each other. Applying this result to pointed strand types of length 2, we now see that P_σ is a convex polygon provided that σ is based on an arc of length 2.

Now, suppose that $\sigma = [(X, x)]$ where X has length at least 3. From the preceding remarks it suffices to consider the case when x is an interior vertex of X . But then we find two shorter pointed strands (X_1, x) and (X_2, x) such that $X = X_1 \cup X_2$. Letting σ_j be the pointed strand type of (X_j, x) , we clearly have $P_\sigma = P_{\sigma_1} \cap P_{\sigma_2}$. By induction, each P_{σ_j} is a small convex polygon. Hence, so is P_σ is a small convex polygon.

We turn now to the second statement of the lemma. If $\sigma = [(A, a)]$ then $\Psi(x) \in P_\sigma$ by definition. Now for the converse. Suppose that the converse is true for some pointed strand type $\sigma_1 = [(X, x_1)]$ and we want to prove it for the pointed strand type $\sigma_2 = [(X, x_2)]$ where x_1 and x_2 are adjacent vertices. Let $a_2 \in \mathbf{Z}^2$ be such that $\Psi(a_2) \in P_{\sigma_2}$. Referring to Equation 9, we have

$$P_{\sigma_2} = P_{\sigma_1} + (\phi^{-4}\epsilon_1 + \phi^{-1}\epsilon_2, \phi^{-3}\epsilon_1).$$

But now let

$$a_1 = a_2 - (\epsilon_1, \epsilon_2).$$

Then by construction $\Psi(a_1) \in P_{\sigma_1}$. Hence there is some arc A such that $[(X, x_1)] = [(A, a_1)]$. But then $[(X, x_1)] = [(A, a_2)]$. So, if the second part of this lemma is true for σ_1 then it is also true for σ_2 . In particular, this lemma is true when σ has length 2.

For the induction step, we can assume that $\sigma = [(X, x)]$, where X has length at least 3 and x is an interior vertex. Then we can write $P_\sigma = P_{\sigma_1} \cap P_{\sigma_2}$ where $\sigma_j = [(X_j, x)]$, as in the previous result. If $\Psi(a) \in P_\sigma$ then $\Psi(a) \in P_{\sigma_j}$. Hence $[(X_j, x)] = [(A_j, a)]$ by induction. But then $\sigma = [(A, a)]$, where $A = A_1 \cup A_2$. ♠

Remark: Our proof suggests a practical method for computing P_σ . The method, which is implemented in Billiard King, simply involves translating and intersecting the tiles of \mathcal{P} according to the combinatorics of σ . The reader familiar with polygon exchange maps will recognize this as the method of pulling back the partition by the dynamics.

3.2 Inflation Maps

In this section and the next we build some machinery for describing the interaction between the dilation map

$$D(x, y) = (\phi^3 x, \phi^3 y)$$

and the map $\Psi : \mathbf{Z}^2 \rightarrow T^2$ given in Equation 7. That is,

$$\Psi(x, y) = \left[(\phi^{-4}x + \phi^{-1}y, \phi^{-3}x) + \frac{1}{2}(\phi^{-3}, \phi^{-2}) \right].$$

Our goal is to define, in a canonical way, a kind of integral approximation to D . Such approximations are vital to the creation of an inflation structure.

We say that a *small polygon* is a convex polygonal subset of T^2 , contained entirely inside an open square of sidelength $1/2$. This technical restriction arises only in the proof of Lemma 3.7 below. We say that a map $\gamma : P \rightarrow T^2$ is a *real similarity* if, relative to local Euclidean coordinates on P and $\gamma(P)$ the map γ is just multiplication by $-\phi^{-3}$. Put another way, γ is a holomorphic map on P whose complex derivative is constantly equal to $-\phi^{-3}$.

let P be a small polygon. Define

$$\Sigma(P) = \Psi^{-1}(P) \cap \mathbf{Z}^2. \quad (10)$$

We say that a map $\beta : \Sigma(P) \rightarrow \mathbf{Z}^2$ is an inflation map if

$$\Psi(\beta(a)) = \gamma(\Psi(a)); \quad \forall a \in \Sigma(P), \quad (11)$$

for some special similarity $\gamma : P \rightarrow T^2$. In the next section we prove the existence of such maps. Here we investigate some of their abstract properties.

Lemma 3.2 *Suppose that β is an inflation map defined relative to P . Let $\hat{\beta}$ be the new map defined by the equation $\hat{\beta}(a) = \beta(a) + b_0$ for some $b_0 \in \mathbf{Z}^2$. Then $\hat{\beta}$ is also an inflation map defined relative to P .*

Proof: We compute that

$$\Psi(\hat{\gamma}(a)) = \Psi(\gamma) + C = \gamma(\Psi(a)) + C = \hat{\gamma}(\Psi(a)).$$

Here C is some constant and $\hat{\gamma}$ is some other special similitude which differs from γ only by a translation. Our equation makes sense because $T^2 = \mathbf{R}^2/\Lambda$ is canonically an abelian group. ♠

Lemma 3.3 *Suppose that β is an inflation map defined relative to P . Given $a_0 \in \mathbf{Z}^2$ let $\widehat{P} = P + \Psi(a_0)$. Define $\widehat{\beta} : \Sigma(\widehat{P}) \rightarrow \mathbf{Z}$ as $\widehat{\beta}(a) = \beta(a - a_0)$. Then $\widehat{\beta}$ is an inflation map defined relative to \widehat{P} .*

Proof: If $a \in \Sigma(\widehat{P})$ then $\Psi(a) \in \widehat{P}$. But then $\Psi(a - a_0) = \Psi(a) - \Psi(a_0) \in P$. Thus $\beta(a - a_0)$ is always defined. We compute

$$\Psi(\widehat{\beta}(a)) = \Psi(\beta(a - a_0)) = \Psi(\beta(a)) - C = \gamma(\Psi(a))$$

for some constant C . The rest of the proof is as in the previous lemma. ♠

Lemma 3.4 *Let β_1 and β_2 be two inflation maps defined relative to the same polygon P . If $\beta_1(a) = \beta_2(a)$ for some $a \in \Sigma(P)$ then $\beta_1 = \beta_2$.*

Proof: Let γ_j be such that $\gamma_j(\Psi(a)) = \Psi(\beta_j(a))$. Note that γ_1 and γ_2 must differ by a translation. Thus, these two maps are equal if they agree at any point. But $\gamma_1(\Psi(a)) = \Psi(\beta_1(a)) = \Psi(\beta_2(a)) = \gamma_2(\Psi(a))$. Hence $\gamma_1 = \gamma_2$. Now we know that $\Psi(\beta_1(a)) = \Psi(\beta_2(a))$ for all $a \in \Sigma(P)$. To finish our proof, we note that Ψ is pretty obviously injective on \mathbf{Z}^2 . ♠

Now we lay the groundwork for explaining how β is an integral approximation to D . Given an inflation map β defined relative to P and $a \in \Sigma(P)$, let

$$v_\beta(a) = D(a) - \beta(a). \quad (12)$$

Here v_β measures the discrepancy between β and the dilation D . Say that β is K -pseudo-Lipschitz if

$$\|v_\beta(a_1) - v_\beta(a_2)\| \leq K \|\Psi(a_1) - \Psi(a_2)\|. \quad (13)$$

Lemma 3.5 *Suppose that the inflation map β , defined relative to P , is K -pseudo-Lipschitz. Then any inflation map $\widehat{\beta}$ defined relative to P is K -pseudo-Lipschitz.*

Proof: In light of Lemma 3.4, we must have, for all $a \in \Sigma(P)$, the identity. $\widehat{\beta}(a) = \beta(a) + a_0$ for some $a_0 \in \mathbf{Z}^2$. The result is obvious from this identity. ♠

3.3 The Shadow Lemma

Recall that convex polygon $P \subset T^2$ is *small* if P is contained inside an open square of radius $1/2$ in T^2 . The polygons P_1, \dots, P_{23} in the partition \mathcal{P} are small.

Lemma 3.6 (Shadow) *Let P be a small polygon. There exists an 4-pseudo-Lipschitz inflation map β defined relative to P .*

It suffices to prove the Shadow Lemma for the map

$$\psi(x, y) = \left[\left(\phi^{-4}x + \phi^{-1}y, \phi^{-3}x \right) \right]$$

which differs from Ψ by a translation of T^2 . That is, we will produce a special similarity γ such that $\psi(\beta(a)) = \gamma(\psi(a))$ for all $a \in A$.

Given that P is small, there are intervals $I_1, I_2 \subset \mathbf{R}$, each having length less than $1/2$ with the following property: For $a = (x, y) \in A$, we have unique integers m and n such that

$$\phi^{-4}x + \phi^{-1}y = m + \epsilon_1; \quad \phi^{-3}x = n + \epsilon_2; \quad \epsilon_j \in I_j. \quad (14)$$

We write $x \sim x'$ if $x - x' \in \mathbf{Z}$. Since $\phi^3 \sim \phi^{-3}$ we have

$$\phi^3x \sim \epsilon_2. \quad (15)$$

Since $2\phi^{-4} + 3\phi^{-3} \sim 0$ and $\phi^3 \sim 2\phi^{-1}$ we have

$$\phi^3y \sim 2\phi^{-1}y \sim 2\epsilon_1 + 3\epsilon_2. \quad (16)$$

Accordingly we define

$$\beta(x, y) = (\hat{x}, \hat{y}); \quad \hat{x} = \phi^3x - \epsilon_2; \quad \hat{y} = \phi^3y - 2\epsilon_1 - 3\epsilon_2. \quad (17)$$

By construction $(\hat{x}, \hat{y}) \in \mathbf{Z}^2$.

Lemma 3.7 *For any $a_1, a_2 \in \Sigma(P)$ we have*

$$\|v(a_1) - v(a_2)\| < 4\|\Psi(a_1) - \Psi(a_2)\|.$$

Proof: Identifying Q with a square in \mathbf{R}^2 we can take local isometric coordinates so that $\psi(a_j) = (\epsilon_{j1}, \epsilon_{j2})$, where ϵ_{j1} and ϵ_{j2} are the constants associated to a_j in Equation 14. Then $\psi(a_1) - \psi(a_2) = V$, where

$$V = (\epsilon_1, \epsilon_2); \quad \epsilon_j = \epsilon_{2j} - \epsilon_{1j}.$$

But then

$$v(a_2) - v(a_1) = MV; \quad M = \begin{bmatrix} 0 & -1 \\ -2 & -3 \end{bmatrix}.$$

In general, a square matrix $\{M_{ij}\}$ expands Euclidean distances by at most

$$\|M\| = \sqrt{\sum_{ij} M_{ij}^2}.$$

When M is the matrix above, we have $\|M\| = \sqrt{14} < 4$. ♠

It is immediate from the definitions that

$$\phi^{-3}\hat{x} \sim -\phi^{-3}\epsilon_2. \quad (18)$$

Lemma 3.8 $\phi^{-4}\hat{x} + \phi^{-1}\hat{y} \sim -\phi^{-3}\epsilon_1$.

Proof: This is a direct computation. To help make the computation easier to understand, we bracket the terms in each line that we replace in the subsequent line by new expressions.

$$\begin{aligned} \phi^{-4}\hat{x} + \phi^{-1}\hat{y} &\sim \phi^{-1}x + (\phi^2y) - \phi^{-4}\epsilon_2 - 2\phi^{-1}\epsilon_1 - 3\phi^{-1}\epsilon_2 \sim \\ &\phi^{-1}x + (\phi^{-1}y) - \phi^{-4}\epsilon_2 - 2\phi^{-1}\epsilon_1 - 3\phi^{-1}\epsilon_2 \sim \\ &(\phi^{-1}x - \phi^{-4}y) + \epsilon_1 - \phi^{-4}\epsilon_2 - 2\phi^{-1}\epsilon_1 - 3\phi^{-1}\epsilon_2 \sim \\ &(2\phi^{-3}) + \epsilon_1 - \phi^{-4}\epsilon_2 - 2\phi^{-1}\epsilon_1 - 3\phi^{-1}\epsilon_2 \sim \\ &(\epsilon_1 - 2\phi^{-1}\epsilon_1) + (2\epsilon_2 - 3\phi^{-1}\epsilon_2 - \phi^{-4}\epsilon_2) \sim -\phi^{-3}\epsilon_1. \end{aligned}$$

This completes the proof ♠

Equation 18 and Lemma 3.8 together immediately show that $\psi(\hat{x}, \hat{y}) = -\phi^{-3}\psi(x, y)$ in local isometric coordinates. This is what we wanted to prove. This completes the proof of the Shadow Lemma.

3.4 Inflation Maps and Dynamical Polygons

Now we put together the material from the previous two sections. The result we prove here, an immediate consequence of what we have already done, provides the key step in constructing a coherent inflation structure from a finite amount of computational information.

Let σ_1 and σ_2 be two pointed strand types. Let Y_{σ_1} and Y_{σ_2} be the associated dynamical polygons. We write

$$\sigma_1 \longrightarrow_{\beta} \sigma_2 \tag{19}$$

if there is an inflation map β , defined relative to Y_{σ_1} having the property that

$$\gamma(Y_{\sigma_1}) \subset Y_{\sigma_2}. \tag{20}$$

Here γ is the special similarity associated to β . The following lemma is really our key result, even though it is a fairly immediate consequence of our previous results.

Lemma 3.9 *Suppose $\sigma_1 \longrightarrow_{\beta} \sigma_2$ and a_1 is that such that $\sigma_1 = [(A_1, a_1)]$ for some polygonal arc A_1 . Then there exists a polygonal arc $A_2 \subset \Gamma$ such that $\sigma_2 = [(A_2, a_2)]$ and $a_2 = \beta(a_1)$.*

Proof: We have $a_1 \in \Sigma(Y_{\sigma_1})$ by the Dynamical Polygon Lemma. By definition $\Psi(a_2) = \gamma(a_1) \subset Y_{\sigma_2}$. By the Dynamical Polygon Lemma we have $\sigma_2 = [(A_2, a_2)]$ for some arc A_2 . ♠

Now we turn our attention to the genes we discussed at the end of §2. Recall that a *gene* is a polygonal arc of length 6 contained in Γ_0 . Here Γ_0 is the component of Γ that contains $(0, 0)$. Each gene A gives rise to a pointed strand (A, a) where a is the central vertex of A . Each gene A_j therefore gives rise to the dynamical polygon Y_j associated to the pointed strand type $[(A_j, a_j)]$. It turns out that there are 75 such dynamical polygons, corresponding to 75 distinct combinatorial types of gene. Figure 4.1 shows these polygons. One can see easily from the picture, or from inspecting the list in §8.1, that any two points in the same dynamical polygon Y_j are within $1/4$ of each other.

3.5 The Inflation Generator

We say that A is *nicely shadowed* by a polygonal arc A' if there is a vertex a' of A' such that the following is true:

- There exists an inflation map β with the properties that $\beta(a) = a'$ and $[(A, a)] \xrightarrow{\beta} [(A', a')]$.
- Let b be one of the endpoints of B . Then one of the endpoints of A' is within 3 units of $D(b)$. (3 is a convenient approximation to the actual bound we compute.)

It turns out that there are 75 different gene types. Compare Figure 4.1. We say that an *inflation generator* is a list G of pairs of the form $\{(A_i, A'_i)\}$ such that each gene of Γ_0 is translation equivalent to one gene A_i on the list, and $A'_i \subset \Gamma$ nicely shadows A_i .

Let A be some gene. There is some gene A_j on our list such that A and A_j have the same type. Let a be the central vertex of A and let a_j be the central vertex of A_j . Let β_j , A'_j , and a'_j be the objects associated to A_j , as above. From Lemma 3.9 there is a pointed strand (A', a') such that $[(A'_j, a'_j)] = [(A', a')]$ and $a' = \beta_j(a)$. We let $\chi(A) = A'$.

Lemma 3.10 χ is an inflation structure.

Proof: For an arbitrary gene A , with gene core B , we need to show that each endpoint of $\chi(A)$ is within 4 units of the corresponding endpoint of $D(B)$. We write $A' = \chi(A)$. Let b be one of the endpoints of B . For ease of labelling let's assume that A_1 is the gene on our list of 75 that has the same type as A . Let B_1 be the core of A_1 and let b_1 be the vertex of B_1 corresponding to B . Let β be the inflation map associated to A_1 . Let b'_1 be the endpoint of A'_1 that is within 3 units of $B(b_1)$. Let Y_1 denote the dynamical polygon associated to $[(A_1, a_1)]$ and let \widehat{Y}_1 be the dynamical polygon associated to $[(A_1, b_1)]$. Note that Y_1 and \widehat{Y}_1 are translates of each other.

Consider a new map $\widehat{\beta}$ defined by the rule

$$\widehat{\beta}(x) = \beta(x + a_1 - b_1) + b'_1 - a'_1$$

By Lemmas 3.2 and 3.3, together with the fact that \widehat{Y}_1 is the relevant translate of Y_1 , we see that $\widehat{\beta}$ is a shadow map defined on $\Sigma(\widehat{Y}_1)$. By the Shadow Lemma

β is 4-pseudo-Lipschitz, and hence so is $\widehat{\beta}$. By translation equivalence, we have $a - b = a_1 - b_1$ and $a' - b' = a'_1 - b'_1$. Therefore

$$\widehat{\beta}(b) = \beta(b' + a_1 - b_1) + b'_1 - a'_1 = \beta(b + a - b) + b' - a' = b'.$$

Note that

$$\|v_{\widehat{\beta}}(a_1)\| = \|b'_1 - D(b_1)\| < 3$$

Therefore

$$\begin{aligned} \|b' - D(b)\| &= \|v_{\widehat{\beta}}(b')\| \leq \|v_{\widehat{\beta}}(b)\| + \|v_{\widehat{\beta}}(b') - v_{\widehat{\beta}}(b)\| < \\ &3 + 4 \operatorname{diam}(Y_1) < 3 + 4(1/4) = 4. \end{aligned}$$

The 1/4 in this last calculation comes from the fact that any two points in the same dynamical polygon are within 1/4 of each other. ♠

3.6 Coherence

Here we explain how to check that the inflation structure χ is coherent. Our inflation generator gives rise to a list $\beta_1, \dots, \beta_{75}$ of shadow maps, where β_j is defined on $\Sigma(Y_j)$. Here Y_j is the dynamical polygon associated to $[(A_j, a_j)]$.

Say that an *extended gene* is a polygonal arc of Γ having length 7. An extended gene is just the union of two consecutive genes. Say that an *extended gene type* is an equivalence class, up to translation, of extended genes. It turns out that there are 89 extended gene types. Given an extended gene X we define $\chi(X) = \chi(X_1) \cup \chi(X_2)$, where X_1 and X_2 are the two genes comprising X .

Lemma 3.11 (Coherence) *Suppose there is a list X_1, \dots, X_{89} of extended genes, representing all the types, such that $\chi(X_j)$ is a polygonal arc for all $j = 1, \dots, 89$. Then χ is coherent.*

Proof: Let \widehat{X} be an arbitrary extended gene. We just need to show that $\chi(\widehat{X})$ is a polygonal arc. After relabelling we can assume that X is the extended gene on our list which is equivalent to \widehat{X} . For each object Y we associate to X let \widehat{Y} be the corresponding object for \widehat{X} .

Let X_1 and X_2 be the two genes comprising X . Let x_1 and x_2 be the two center points of these genes. Let β_1 and β_2 be the inflation maps associated to the gene types of X_1 and X_2 . Suppose we knew that

$$\beta_1(\hat{x}_1) - \beta_2(\hat{x}_2) = \beta_1(x_1) - \beta_2(x_2). \quad (21)$$

Then the two strands $\chi(\widehat{X}_1)$ and $\chi(\widehat{X}_2)$ are in the same relative positions as the strands $\chi(X_1)$ and $\chi(X_2)$. Hence, Equation 21 implies this lemma.

Since Ψ is injective on \mathbf{Z}^2 it suffices to show that

$$\Psi(\beta(\hat{x}_1)) - \Psi(\beta(\hat{x}_2)) = \Psi(\beta(x_1)) - \Psi(\beta(x_2)). \quad (22)$$

Let $p_j = \Psi(x_j)$ and $\hat{p}_j = \Psi(\hat{x}_j)$. We know that

$$\hat{x}_1 - x_1 = \hat{x}_2 - x_2$$

because there is a translation carrying \widehat{X} to X . Therefore, setting $p_j = \Psi(x_j)$ and $\hat{p}_j = \Psi(\hat{x}_j)$, we have

$$\hat{p}_1 - p_1 = \hat{p}_2 - p_2.$$

Let $\gamma_j : Y_j \rightarrow T^2$ be the similarity associated to β_j . Since γ_1 and γ_2 are local similarities which agree up to translations, we have

$$\gamma_1(\hat{p}_1) - \gamma_1(p_1) = \gamma_1(\hat{p}_1 - p_1) = \gamma_2(\hat{p}_2 - p_2) = \gamma_2(\hat{p}_2) - \gamma_2(p_2).$$

Rearranging this, we have

$$\gamma_1(\hat{p}_1) - \gamma_1(\hat{p}_2) = \gamma_1(p_1) - \gamma_1(p_2). \quad (23)$$

But we also know that

$$\gamma_j(p_j) = \Psi(\beta_j(x_j)); \quad \gamma_j(\hat{p}_j) = \Psi(\beta_j(\hat{x}_j)). \quad (24)$$

Equations 23 and 24 combine to establish Equation 22. ♠

4 Computer Aided Verification

4.1 Overview

Recall that a gene is a polygonal arc of length 6 contained in Γ_0 , the component of the arithmetic graph containing $(0, 0)$. We are trying to verify the existence of an inflation generator. This inflation generator consists of a length 75 list of the form $\{(A_j, A'_j)\}$, where A_j is a gene and A'_j is a path that nicely shadows A_j in the sense of §3.5. We associate some auxiliary objects to our list, namely:

- Let Y_j be the dynamical polygon associated to A_j .
- Let β_j be the inflation map associated to (A_j, A'_j) .
- Let $\gamma_j : Y_j \rightarrow T^2$ be the similarity associated to β_j . Here $\gamma_j \circ \Psi = \Psi \circ \beta_j$, whenever all maps are defined.

Given these basic objects, here are the things we need to check:

1. Each endpoint of A'_j is within 3 units of the corresponding endpoint of B_j , the core of A_j . We have a list of all the vertices involved and we just check this directly. See §9.
2. For each gene A_j , with center vertex a_j , we have correctly computed the dynamical polygons Y_j associated to $[(A_j, a_j)]$.
3. We have $\gamma_j(Y_j) \subset Y'_j$, where Y'_j is the dynamical polygon associated to the pointed strand type $[(A'_j, a'_j)]$. Our method will not require us to compute P'_j explicitly.
4. There is a complete list X_1, \dots, X_{89} of representatives of extended genes such that $\chi(X_j)$ is a polygonal arc for $j = 1, \dots, 89$. Here *complete list* means that every extended gene type is represented.
5. Our list A_1, \dots, A_{75} of gene types is exhaustive and our list X_1, \dots, X_{89} of extended gene types is exhaustive. There are no other gene types or extended gene types.

In this chapter we will explain the main theoretical points of our verifications. In §9 we will write enough pseudo-code so that the interested reader can see explicitly how we do all the calculations.

4.2 Computing the Polygons

Let $A = A_j$ denote one of the genes on our list. Let a_{-2}, \dots, a_2 denote the 5 interior vertices of A . We are interested in computing the dynamical polygon Y associated to the pointed strand type $[(A, a_0)]$. Billiard King computes these polygons using the method suggested after the proof of the Dynamical Polygon Lemma in §3.1. Here we will discuss this method in more detail.

We define a *dynamical translation* of the torus T^2 to be a map of the form

$$[(x, y)] \rightarrow [(x, y) + (\epsilon_1\phi^{-4} + \epsilon_2\phi^{-1}, \epsilon\phi^{-3})]; \quad \epsilon_1, \epsilon_2 \in \{-1, 0, 1\}. \quad (25)$$

This operation makes sense because $T^2 = \mathbf{R}^2/\mathbf{Z}^2$ is canonically an abelian group. We remind the reader that $[(x, y)]$ is the equivalence class of the point (x, y) in T^2 . We say that (ϵ_1, ϵ_2) is the *type* of the dynamical translation.

As associate to A a list Q_{-2}, \dots, Q_2 of 5 polygons of the partition \mathcal{P} . For this discussion we take these polygons to be open. They do not contain their boundaries. Here Q_j is the polygon having the same local type as the vertex a_j . Depending on A there are 4 dynamical translations T_{-2}, T_{-1}, T_1, T_2 with the property that $x \in Y$ if and only if

- $x \in Q_0$.
- $T_1(x) \in Q_1$
- $T_2(T_1(x)) \in Q_2$.
- $T_{-1}(x) \in Q_{-1}$.
- $T_{-2}(T_{-1}(x)) \in Q_{-2}$.

We call these four conditions *Property X*. Given this information we have

$$Y = Q_0 \cap T_1^{-1}(Q_1 \cap T_2^{-1}(Q_2)) \cap T_{-1}^{-1}(Q_{-1} \cap T_{-2}(Q_2)). \quad (26)$$

Billiard King simply computes this double intersection.

If we replace each set Q_j by its closure \overline{Q}_j , then we arrive at a criterion for when $x \in \overline{Y}$. We call this criterion *Property \overline{X}* .

Figure 4.1 shows the 75 dynamical polygons in dark grey. We list the actual coordinates in §8.2. The 24 light polygons comprise the complement. Here is their interpretation: A vertex p in the arithmetic graph lies on a closed polygon of length 5 or 7 if and only if $\Psi(p)$ lies in the interior of one of

the light polygons. We do not use these light polygons in this paper, but we note that they “round out” Figure 4.1 by explaining what is left over after we plot our 75 dynamical polygons.

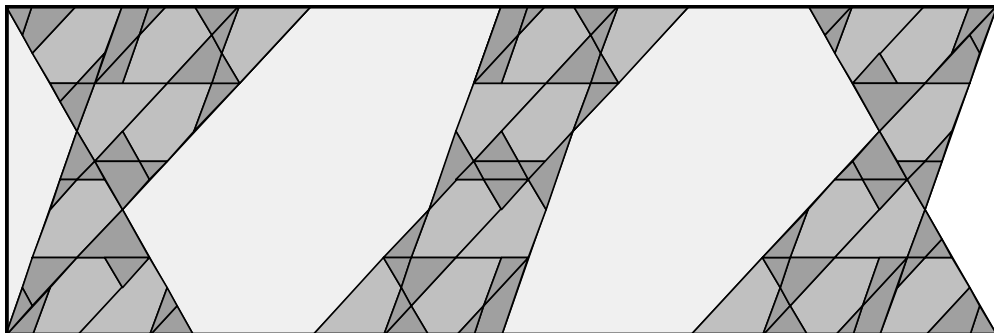


Figure 4.1: The partition

For the first stage of our verification, we use the Billiard King algorithm to compute Y to high precision. Next, we use the fact that the vertices of Y are elements of $\frac{1}{2}\mathbf{Z}[\phi]$ to guess the exact expression for the vertices. Let Y_G denote this guess. Our goal is simply to verify that $Y_G = Y$.

First we check that each vertex of Y_G satisfies Property \overline{X} . This tells us that $\overline{Y_G} \subset \overline{Y}$. If $\overline{Y_G}$ is a property subset of \overline{Y} then there is some edge e of Y_G such that every point x on the interior of e satisfies Property X . We rule this out by explicitly choosing one point per each edge of GP and showing that it fails to have Property X . In §9 we explain the calculation in detail.

When we run the computation for each of the 75 cases it works. Of course, the fact that Figure 4.1 is a partition of the torus gives extremely strong visual evidence that we have guessed correctly in the first place.

4.3 Checking the Shadowing Property

Our method here is quite similar to our method for verifying that $Y_G = G$. Let $A = A_j$ be one of our genes. Let $\beta = \beta_j$, etc. be the objects associated to A . Our goal is to check that $\gamma(Y) \subset Y'$.

Let $Q'_{-1}, Q'_0, Q'_1, \dots$ be the sequence of polygons in the partition \mathcal{P} associated to the vertices of A' . We set up the indices so that the 0th vertex of A' is the distinguished point a' that shadows $D(a)$. (Here a is the center of the gene A .)

Just as we did for A , we generate the sequence of dynamical translations for the strand A' . This is a sequence whose length varies with the choice of

gene. The length typically varies from 10 to 20. The condition that $x \in Y'$ amounts to checking that x satisfies what we call *Property X'* :

- $x \in Q'_0$.
- $T_1(x) \in Q'_1$ and $T_{-1}(x) \in Q'_{-1}$
- $T_2(T_1(x)) \in Q'_2$ and $T_{-2}(T_{-1}(x)) \in Q'_{-2}$
- $T_3(T_2(T_1(x))) \in Q'_3$ and $T_{-3}(T_{-2}(T_{-1}(x))) \in Q'_{-3}$
- etc.

We also have the corresponding Property $\overline{X'}$, the closed version. We simply check that each vertex of $\gamma(Y)$ satisfies Property $\overline{X'}$. This means that the closure of $\gamma(Y)$ is contained in the closure of Y' . Hence $\gamma(Y) \in Y'$. Billiard King computes all these quantities and displays them visually so that the user can see in each case that $\gamma(Y) \subset Y'$.

4.4 Checking the Coherence

We will use the forwards direction of Γ_0 to check the coherence. In order to make the construction to follow we first need to know something about a certain finite portion of Γ_0 . We verify by direct inspection that Γ_0 contains a polygonal arc of combinatorial length 2^{14} , connecting $(0, 0)$ to a point in the positive quadrant.

In this section we will use the notation and terminology from §3.6 and the Coherence Lemma. In particular X_1, \dots, X_{89} is a complete list of representatives of the extended gene types.

For $N \leq 13$ let Γ_0^N denote the first 2^N segments of Γ_0 , starting from $(0, 0)$ and moving in the direction of the positive quadrant.. We call N *sufficiently large* if each extended gene type has a representative on Γ_0^N . We show by a direct computation that $N = 10$ is sufficiently large. Once we have our list of 89 gene types it is a completely straightforward matter of checking that they all occur on Γ_0^{10} . *A fortiori*, the polygonal arc Γ_0^{10} contains each of our genes A_1, \dots, A_{75} .

Our inflation generator gives rise to the inflation structure χ . Our goal is to prove that χ is coherent. Here is the strategy. Given any gene $A \subset \Gamma_0^{10}$, we let a be the center point of A . We know that A has the same gene type

as some gene A_j in our inflation generator. The center point a_j of A_j is such that $D(a_j)$ is close to the point $\beta_j(a_j)$. We record the gene type of the gene centered at $\beta_j(a_j)$ and then find a point $a' \in \Gamma_0^{13}$ which is near $D(a)$. We then verify by direct computation that $\beta_j(a) = a'$.

Now we know that $\chi(A) \subset \Gamma_0$. We check explicitly that the points a'_1, \dots, a'_{1024} occur in order on Γ_0^{13} . This means that the two strands $\chi(A_1)$ and $\chi(A_2)$ overlap whenever A_1 and A_2 are consecutive genes on Γ_0^{10} . But then $\chi(A_1) \cup \chi(A_2)$ is a polygonal arc. This works for all consecutive genes on Γ_0^{10} , including the 89 we need for the Coherence Lemma. Applying the Coherence Lemma, we see that χ is coherent. See §9 for more details.

4.5 Checking the Completeness of the Lists

We compute explicitly that Γ_0^{10} contains 75 gene types and 89 extended gene types. We also compute explicitly that Γ_0^{13} has 75 gene types and 89 extended gene types. That is, when we go out 8 times as far, we see no new genes or gene types. We also recall that Γ_0^{10} is shadowed by a subset of Γ_0^{13} . This means that the process of replacing A_j by $\chi(A_j)$, for each of $j = 1, \dots, 75$ produces no new gene types and no new extended gene types. Iterating, and applying induction we see that our list of gene types and extended gene types is complete, in the forwards direction. We then make all the same checks in the backwards direction.

Remark: We could take an entirely different approach to the completeness of our list of genes based on Figure 4.1. Figure 4.1 shows a partition of the grey polygons of \mathcal{P} into 75 light grey polygons and 24 dark grey polygons. As we mentioned above, the dark grey polygons correspond to points in the arithmetic graph contained on closed 5-gons or closed 7-gons. Our list of genes is complete because the remaining part of \mathcal{P} is completely partitioned by the 75 corresponding dynamical polygons. Any additional gene type would have a dynamical polygon that overlaps with one of the ones we already have plotted. We do not insist on this approach because it requires an analysis of the 24 dark gray polygons in the picture, something we have not attempted. A similar picture would reveal the completeness of the list of 89 extended gene types.

5 Proof of Theorem 1.2

5.1 Existence of the Orbits

For starters, we show that the orbits of points in C^* are entirely defined. Since the vertices of our shape S lie in $\mathbf{Z}[\phi]$, the outer billiards map is defined on and preserves $(\mathbf{R} - 2\mathbf{Z}[\phi]) \times \mathbf{Z}'$. (Compare the proof of Lemma 2.1.) So, to show that the orbits of points in C^* are entirely defined, it suffices to prove that $C^* \cap 2\mathbf{Z}[\phi] = \emptyset$.

Suppose there is some $x = a + b\phi \in C^*$, with $a, b \in 2\mathbf{Z}$. We take $|a| \geq 2$ as small as possible. Let C_L^* and C_R^* denote the left and right halves of C^* .

Case 1: Suppose $x \in C_L^*$. Then $\phi^3 x \in C^*$ and $\phi^3 x = (a + 2b) + (2a + 3b)\phi$. Suppose that $a > 0$. Then, by minimality, $|a + 2b| \geq a$. If $a + 2b \geq a$ then $2b \geq 0$, but then $a + b\phi \geq a \geq 1$ and $x \notin C$. If $a + 2b \leq -a$ then $b \leq -a$ and $a + b\phi \leq a(1 - \phi) < 0$ and $x \notin C$. Either case leads to a contradiction.

Suppose that $a < 0$. If $a + 2b \leq a$ then $2b \leq 0$ and $a + b\phi < 0$ and $x \notin C$. If $a + 2b \geq -a$ then $b \geq -a$ and $a + b\phi \geq (-a)(-1 + \phi) \geq \phi^{-1} \notin C$.

Case 2: Suppose $x \in C_R^*$. Then $\alpha(x) \in C^*$, where $\alpha(y) = \phi^3 y + 2\phi^{-3} - 2$. (This map preserves the right endpoint $2\phi^{-3}$ of C .) We compute

$$\alpha(x) = (a + 2b) + (2a + 3b)\phi + (-6 + 4\phi) - 2 = (a + 2b - 8) + (2a + 3b + 4)\phi.$$

Suppose $a > 0$. We know $|a + 2b - 8| \geq a$. If $a + 2b - 8 \geq a$ then $2b \geq 8$ and $a + b\phi > a \geq 1$ and $x \notin C$. If $a + 2b - 8 \leq -a$ then $2b - 8 \leq -2a$ and $b \leq 4 - a$. Given that $b \leq 4 - a$ we have

$$0 < x \leq a + (4 - a)\phi = 4\phi - a\phi^{-1}.$$

This forces $a < 4\phi$. The only choices are $a = 2, 4, 6$. But there is no choice for $b \in 2\mathbf{Z}$ which places $a + b\phi$ in $[0, 2\phi^{-3}]$ for any of these 3 choices of a .

Suppose $a < 0$. Since $a < 0$ and $a + b\phi > 0$ we must have $b > 0$. If $a + 2b - 8 \leq a$ then $b = 2, 4$. No choice of $a \in 2\mathbf{Z}$ places $a + 2\phi$ or $a + 4\phi$ in C^* . If $a + 2b - 8 \geq -a$ then $b \geq 4 - a$. But then

$$a + b\phi \geq a + (4 - a)\phi \geq (-a)(\phi - 1) + 4\phi > 1.$$

Hence $x \notin C$.

This takes care of all the cases.

5.2 A Gap Phenomenon

Let Γ_- denote the backwards half of Γ_0 . In trying to propagate the pulsing property of Γ_- , we might worry that the approximate nature of the self-similarity of Γ_- causes the “lowest points approach” to slowly drift away from ∂H . A certain *gap phenomenon* comes to the rescue.

Let

$$\psi(x) = \left[\left(\frac{x}{2\phi}, \frac{x}{2} \right) \right].$$

Recall that $\Psi = \psi \circ T$. Recall that P_1, \dots, P_{26} are the polygons comprising the partition \mathcal{P} of T^2 . The polygon P_3 is the parallelogram at the bottom left of Figure 2.5. The segment $\psi([0, 2\phi^{-3}])$ is the long diagonal of P_3 . In the result that follows (and everywhere else in the paper) we consider P_3 as an open polygon.

Lemma 5.1 *Suppose that $x \in (0, 16)$ and $\psi(x) \in P_3$. Then $x \in (0, 2\phi^{-3})$.*

Proof: Looking at Figure 2.5 we see that P_3 is the little parallelogram in the bottom left corner. The corner vertex of P_3 is $(0, 0)$ and the opposite vertex is (ϕ^{-4}, ϕ^{-3}) . So, if $\psi(x) \in P_3$ then $\delta(x/2) \in (0, \phi^{-3})$. Hence $x \notin [2\phi^{-3}, 2]$. It is now an easy exercise to check that the segment $\psi([2, 16])$ is disjoint from P_3 . One way to do this exercise is to plot the ψ -image of the 2000 maximally and evenly spaced points in the interval $[2, 16]$ and observe that none of them is within .0001 of P_3 . Since ψ is 1-Lipschitz, our plot guarantees that no point of $[2, 16]$ lies in P_3 . We omit the details. ♠

Given a point $p \in H$, the halfplane containing the arithmetic graph, let $v(p)$ denote the length of the vertical line segment connecting p to the line through the origin parallel to ∂H . For instance $v(0, m) = m$.

Corollary 5.2 (Gap Phenomenon) *Suppose p is a point of the arithmetic graph having type 3. If $v(p) < 7$ then $v(p) < \phi^{-3}$.*

Proof: Note that $T(0, 7) < 15$, and the fibers of T are parallel to ∂H . Hence $T(p) \in (0, 15)$. By definition, $\psi(T(p)) \in P_3$. Hence $T(p) \in (0, 2\phi^{-3})$. But $T(0, \phi^{-3}) > 2\phi^{-3}$. In other words, if $v(p') = \phi^{-3}$ then $T(p') > 2\phi^{-3}$. Hence $v(p) < \phi^{-3}$. ♠

5.3 Infinite Return

In this section we prove that $O_-(p)$ returns to every neighborhood of p infinitely often. We think of this as a warm-up to the proof of Theorem 1.2. Let A_0 be the gene through the origin. Let A'_0 be the strand that shadows it. Figure 3.1 shows the picture.

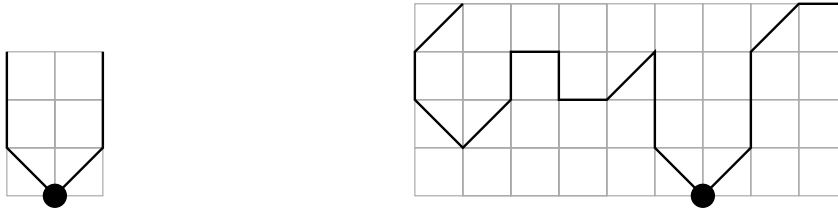


Figure 5.1: The gene A_0 and its shadow A'_0 .

The dynamical polygon Y_0 associated to A_0 is contained in P_3 , because the center of A_0 has type 3. Thus Y_0 is a small tile in the bottom left corner of Figure 2.5. Here we show a plot, and describe all the plotted objects in order of decreasing size. Each polygon is contained in the previous one.

- The big L is the corner of our fundamental domain for T^2 .
- The big parallelogram is P_3 .
- The big triangle is Y_0 .
- The small parallelogram is Y'_0 , the polygon associated to A'_0 .
- The small triangle is $\gamma(Y_0)$, where γ is the special contraction fixing $\Psi(0, 0)$.

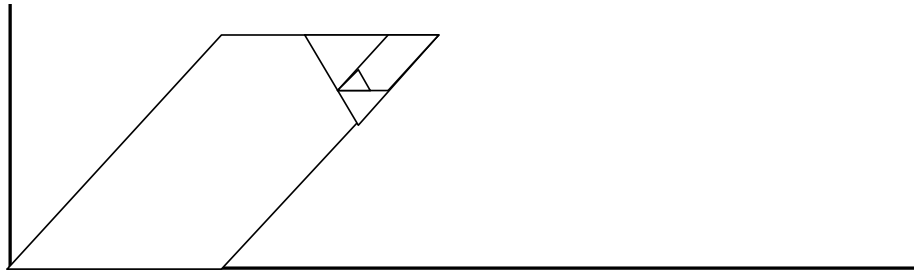


Figure 5.2: The associated dynamical polygons.

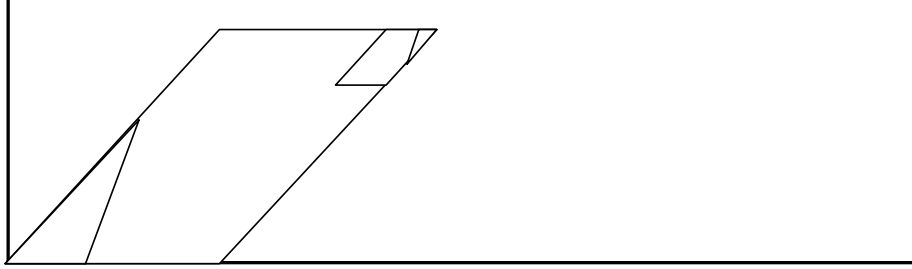


Figure 5.4: The associated dynamical polygons.

We set $K = P_3$ and $K_0 = Y'_0$ and $\gamma_0 = \gamma$. There are several geometric pieces of information we now record. First, $\gamma_0(K) = K_0$. Second, Let a_0 and a_1 be the two type-3 points of A'_0 . For instance, we might take A'_0 such that $a_0 = (0, 0)$ and $a_1 = (-5, 1)$. From Equation 7 we compute that

$$V_0 := \Psi(a_0) - \Psi(a_1) = [(5\phi^{-4} - \phi^{-1}, 5\phi^{-3})] = (\phi^{-4} - \phi^{-7}, \phi^{-3} - \phi^{-6}). \quad (27)$$

Let $\tau(x) = x - V_0$. Geometrically, the translated parallelogram $K_1 = \tau(K_0)$ has $(0, 0)$ as a vertex and fits exactly into the lower left corner of K . Figure 5.5 shows a schematic picture. Let $\gamma_1 = \tau \circ \gamma_0$. Then $\gamma_j(K) = K_j$. We define $K_{00} = \gamma_0(K_0)$ and $K_{01} = \gamma_0(K_1)$, etc. Figure 5.5 shows a schematic picture of the first few of these sets.

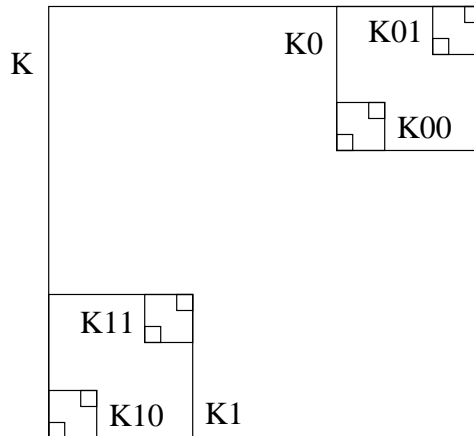


Figure 5.5: A schematic picture

The reader might expect K_{00} to be on the top and K_{11} on the bottom, rather than in the middle. This twisting of the labelling comes from the fact

that γ is orientation reversing. The fixed point of γ is the nested intersection $K_0 \cap K_{00} \cap K_{000} \dots$

Lemma 5.3 *Let Σ be the semigroup generated by γ_0 and γ_1 . Then the closure of any Σ orbit of a point in K is a self-similar Cantor set C' whose endpoints are two opposite vertices of K .*

Proof: This is clear from Figure 5.5. ♠

Now we can explain the Cantor set structure. Suppose that X is a type 3 point Γ_- such that X is the center of a gene A that is a copy of either A_0 or A_1 . Suppose also that $v(X) < \phi^{-3}$. Let X_0 and X_1 be the two points of A' having type 3. Our notation is such that X_0 is the center of a copy of the gene A_0 and X_1 is the center of the copy of the gene A_1 . The point X_0 shadows the dilated point $\phi^3 X$, and the point X_1 is several units to the right. Our arguments above show that

- $v(X_0)$ and $v(X_1)$ are both less than ϕ^{-3} .
- $\Psi(X_1) \subset K_1$ and $\Psi(X_0) \subset K_0$.
- $\tau(\Psi(X_0)) = \Psi(X_1)$.
- $\Psi(X_j) = \gamma_j(\Psi(X))$.

Now we consider a tree-like induction process. We start with the point $X = (0, 0) \in \Gamma_-$. Considering the above inflation process, we produce the points

$$X_0 = X; \quad X_1 = (-5, 1).$$

Inflating again, we produce the points

$$X_{00} = X_0; \quad X_{01} = X_1; \quad X_{10} = (-21, 5); \quad X_{11} = (-26, 5).$$

Inflating again, we produce the 8 points, corresponding to the binary strings of length 3, and so on. In general, we produce one point $X_\beta \in \Gamma_-$ for each finite binary string β . (These points are not all distinct, e.g. $X_{00} = X_0$.) By construction

$$\Psi(X_\beta) \subset K_\beta.$$

Therefore, the closure of $\Psi(\Gamma_-)$ contains the Cantor set C' from Lemma 5.3. (We mean the closure of the vertex set.)

Let $I_0 = [0, 2\phi^{-3}]$. We have already remarked that $\psi(I_0)$ is long diagonal of P_3 , namely the segment that connects the two endpoints of the Cantor set C' . Recall that the map T maps the vertices of Γ_- onto the backwards orbit $O_-(p)$. Also $\Psi = \psi \circ T$. Therefore $C = \psi(C')$, where $C \subset I_0$ is an affine image of C' . By construction C is the Cantor set from Theorem 1.2. (We are identifying $[0, \infty) \times \{-1\}$ with $[0, \infty)$, as discussed at the beginning of the chapter.) We have realized C as a set contained in the closure of $O_-(p)$. In particular $O_-(p)$ returns infinitely often to C .

5.5 2-adic Structure

Since $\psi(I_0)$ is the long diagonal of P_3 we get the following result: If $x \in \mathbf{Z}^2 \cap H$ is such that $T(x) < 2\psi^{-3}$ then x has type 3. We say that $x \in \Gamma_-$ is a *basepoint* if $T(x) \in I_0$.

We see inductively that our shadowing construction accounts for all the basepoints of Γ_- . That is, every such point arises on a strand of Γ_- that shadows an inflated gene. Therefore, we can index the basepoints by binary strings β . Each binary string β represents the integer $n(\beta)$ as usual. For instance

$$n(11001) = (1, 1, 0, 0, 1) \cdot (16, 8, 4, 2, 1) = 25.$$

Examining our construction we see that the two points X_β and $X_{\beta'}$ are equal if and only if $n(\beta) = n(\beta')$. Moreover, as we travel along Γ_- away from $(0, 0)$ we encounter the points X_β in order of the integers they represent!

Let $\theta_2 : \mathbf{Z}_2 \rightarrow C$ be the homeomorphism from Theorem 1.2. By construction, we have $\theta_2(0) = p$. Let $T : \mathbf{Z}^2 \rightarrow [0, \infty)$ be the map from Equation 3. Let X and X_0 and X_1 be the points referred to in our shadowing construction above. We have already mentioned that

$$\Psi(X_0) = \gamma_j(X); \quad j = 0, 1.$$

Given the defining property of θ_2 , we have

$$\theta_2^{-1}(T(X_j)) = 2\theta_2^{-1}(T(X)) + j; \quad j = 0, 1.$$

But then we have

$$\theta_2(T(X_\beta)) = n(\beta).$$

But, by construction $T(X_\beta)$ is the n th point of $O_-(p) \cap I_0$, which is the same as the n th point of $O_-(p) \cap C$. Hence θ_2 maps the n th point of $O_-(p) \cap C$ to n . This is the second statement of Theorem 1.2.

Now we will deal with the question of return times and excursion distances for the points of $O_-(n)$. Given a basepoint X , let $\Gamma_+(X)$ be the forwards portion of Γ_0 which starts at X . Let X and X_0 and X_1 be as in the previous section, so that X_0 is the basepoint that shadows $\phi^3 X$.

By the inflation property, $\Gamma_+(X_0)$ closely follows $\phi^3 \Gamma_+(X)$. Also, one can see by looking at a single example that the initial portion of $\Gamma_+(X_0)$ rises up at least 10 units from ∂H before coming back towards ∂H . Moreover, the next basepoint (after X_0) encountered by $\Gamma_+(X_0)$ is the one that shadows the dilation of the next basepoint encountered by $\Gamma_+(X)$. These properties show that $\Gamma_+(X_0)$ rises up about ϕ^3 times as high as $\Gamma_+(X)$, and takes about ϕ^3 times as long to return to the next basepoint as does $\Gamma_+(X)$. The next basepoint encountered by $\Gamma_+(X_0)$ is the one that shadows the dilation of the next basepoint encountered by $\Gamma_+(X)$. On the other hand, $\Gamma_+(X_1)$ just travels a few units to the right before returning to the basepoint $\Gamma_+(X)$.

Given any binary string β , let $\nu(\beta)$ denote the number of 0s on the right of β . For instance $\nu(11000) = 3$. Equivalently, $\nu(\beta)$ equals the number of powers of 2 dividing $n(\beta)$. Given $X = X_\beta$ let $\nu = \nu_\beta$. Applied inductively, our arguments show that $\Gamma_+(X)$ rises up roughly $\phi^{3\nu}$ units before returning to the next basepoint after roughly $\phi^{3\nu}$ units of time. Here $X = X_\beta$ and ν denotes the number of 0s on the right of β . Hence the excursion distances and return times for the forward orbit of the n th point x_n of $O_-(p) \cap C$ are proper functions of the 2-adic distance from $\theta_2^{-1}(x_n)$ to 0.

By simply reversing the direction of $\Gamma_+(X)$ we see that the excursion distances and return times for the forwards orbit of x_n are proper functions of the 2-adic distance from $\theta_2(x_n)$ to -1 . The point here is that θ_2 maps n and $n - 1$ respectively to the endpoint of $\Gamma_+(\beta)$ and the first basepoint it encounters when travelling to the right.

There is one more observation we want to make. If X is a basepoint and $\nu(X)$ is very large, then a very long initial portion of $\Gamma_+(X)$ looks exactly like $\Gamma_+(0, 0)$, the forward portion of Γ_0 that starts at $(0, 0)$. This is because both strands are “produced” by many iterates of the same inflation process. An equivalent way to see this is that any finite portion of Γ_0 is determined by some small dynamical polygon in T^2 containing $\Psi(0, 0)$. If X is some point with $\nu(X)$ large, then $\Psi(X)$ belongs to this same dynamical polygon.

5.6 Extension to the Cantor Set

Lemma 5.4 (Rising) *Let K be some constant and let X be some basepoint of Γ_- . Then there is some K' with the following property. If we take K' steps in either direction along Γ_- , starting at X , then we rise at least K units above ∂H .*

Proof: Consider the forwards direction. The backwards direction is similar. If this lemma is false then we can encounter a long string of basepoints $\{X_i\}$ such that $\nu(X_i)$ is always small. But the map $x \rightarrow x - 1$, when iterated, brings any point very close 2-adically to 0 within a uniform number of steps. Hence, we don't have to walk very long from X before we hit a basepoint with high ν -value, and then we rise up steadily away from ∂H for a long time. This comes from the fact that a long initial portion of $\Gamma_+(X)$ is a translate of a long initial portion of $\Gamma_+(0, 0)$, as we remarked above. ♠

Lemma 5.5 *The forwards and backwards orbits of $y \in C^*$ are unbounded.*

Proof: We can find a sequence $\{x_n\} \in O_-(p)$ converging to y . For n sufficiently large, the first K' iterates of x_n and y will have the same combinatorial structure. Here $K' \rightarrow \infty$ as $n \rightarrow \infty$. But then the first K' iterates of y remain (say) within 1-unit of the corresponding K' iterates of x_n . Letting K' be as in the Rising Lemma, we see then that some point of x_n rises up K units and therefore some iterate of y rises up at least $K - 1$ units. Since K is arbitrary, the orbit of y (in either direction) is unbounded. ♠

We continue with the notation from the lemma. Let $x_{n,-}$ denote the forward return of the point x_n . As long as $y \not\equiv p$, there is some uniform K such that x_n and $x_{n,1}$ are separated by at most K units. Here K depends on y but not on n . This we see that y_- and t are separated by at most K units. For n large enough the orbit of x_n has the same combinatorial structure as the orbit of y for the first K iterates. Hence $y_- - y = x_{n,-} - x_n$. Therefore, by continuity, $\theta_2^{-1}(y_-) = \theta_2^{-1}(y) - 1$. The same continuity argument takes care of the statement about the return times and excursion distances for the forward orbit. This proves the third statement of Theorem 1.2, and the fourth statement has essentially the same proof.

6 Proof of the Arithmetic Graph Lemma

6.1 Factoring the Return Map

In this section we explore some of the geometry of Υ_R .

Say that a *strip* is a region $A \subset \mathbf{R}^2$ bounded by 2 parallel lines, $\partial_0 A$ and $\partial_1 A$. Let V be a vector such that $\partial_0 S + V = \partial_1 A$. That is, V points from one boundary component to the other. Given the pair (A, V) we (generically) define a map $E : \mathbf{R}^2 \rightarrow A$ as follows. For each generic $x \in \mathbf{R}^2$ we define $E(x) = x - nv$ where n is the unique integer such that $E(x) \in A$. This map is well defined unless x lies in a discrete infinite family of parallel lines.

There is a unique affine functional $f(x, y) = a_1x + a_2y + a_3$ such that $f_L(v) = 1$, and $f(x, y) \in (0, 1)$ iff $(x, y) \in A$. Here $f_L(x, y) = a_1x + a_2y$ is the linear part of f . Given f we have the following explicit formula:

$$E(p) = p - \text{floor}(f(p)) v. \quad (28)$$

Equation 28 is defined unless $f(p)$ is an integer. We say that $\alpha = (a_1, a_2, a_3)$ is the *triple associated to* (A, V) .

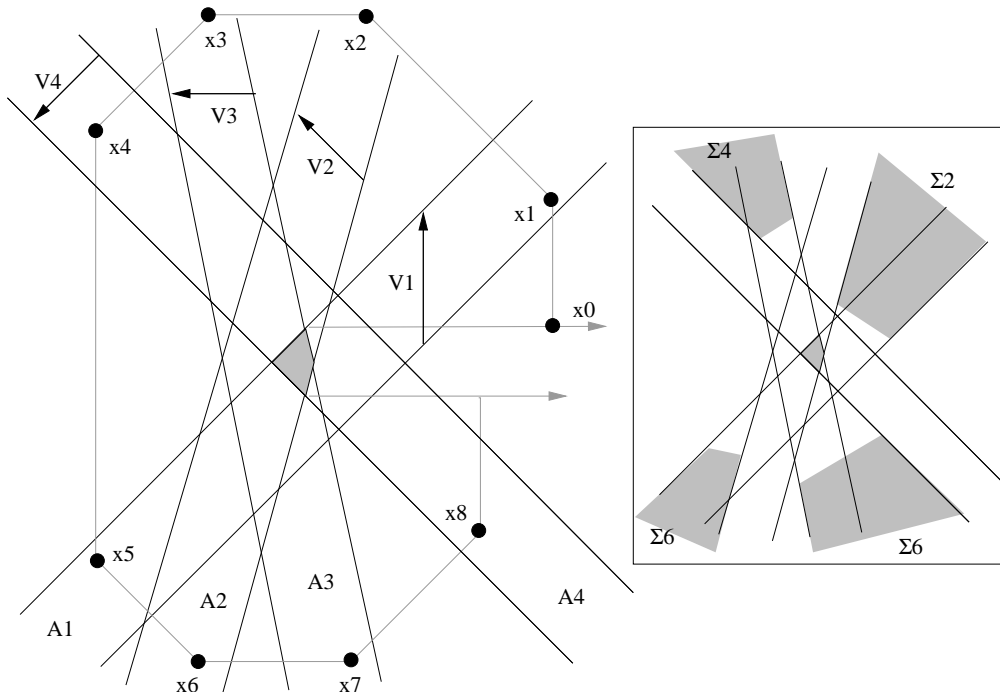


Figure 6.1: The pinwheel

Each strip in Figure 6.1 is obtained by extending an edge of the side of S , and then rotating this extended side through one of the vertices that does not contain the edge. (The choice should be clear from the picture.) We call the strips A_1, A_2, A_3, A_4 . We set $E_j = (A_j, V_j)$ for $j = 1, 2, 3, 4$ and $E_{j+4} = E_j$

Lemma 6.1 (Pinwheel) *Let $x_0 \in \mathcal{C}(\pm)$. Let $x_j = E_j(x_{j-1})$. Then x_8 and $\Upsilon_R(x_0)$ lie on the same vertical line.*

Proof: Let $V_{j+4} = -V_j$ for $j = 1, 2, 3, 4$. For any x on which Υ is defined, we have $\Upsilon(x) - x = V_x$, where V_x is twice one of the vectors pointing from one vertex of S to another. The vectors V_1, \dots, V_8 have this form.

The lines comprising our strips divide \mathbf{R}^2 into a finite number of bounded regions and a finite number of unbounded regions. Let K denote the closure of the union of bounded regions. One can check, with a little experimentation, that the finitely many iterates $p, \Upsilon(p), \dots, \Upsilon_R(p)$ avoid the set K provided that $p = (x_0, \pm 1)$ and $x_0 > 4$. We will consider such points first.

The complement of K is divided into 8 sectors $\Sigma_1, \dots, \Sigma_8$. Each sector Σ_j is bounded by one line of A_{j-1} and one line of A_j , and contains a non-compact subset of A_{j-1} . The right hand side of Figure 6.1 indicates these sectors. It is easy to check that $q \in \Sigma_j$ implies $V_q = V_j$. This result immediately implies our lemma for points $(x_0, \pm 1)$ where $x_0 > 4$ and all maps are defined.

When $x_0 < 4$ we can just check the few cases by hand. Indeed, to be sure we sampled 1 million evenly spaced points in the two intervals $(0, 10) \times \{\pm 1\}$.

♠

The Pinwheel Lemma lets us *factor* the return map. The composition $E_8 \dots E_1$ maps $x_0 \in \mathcal{C}(\pm)$ to $x_8 \in \mathbf{R}^2$, and the y -coordinate of x_8 is $\pm 1 + 4k$. In each case, $\Psi_R(x_0) \in \mathcal{C}(\pm)$. Hence

$$\Upsilon_R = \zeta \circ (E_4 \circ \dots \circ E_1)^2; \quad \zeta(x, \pm 1 + 4k) = (x, \pm 1). \quad (29)$$

Remarks:

(i) We consider it a lucky accident that Equation 29 holds for points near the origin, and we still don't really understand it. For a result like Theorem 1.1, it is clear that mainly we care about Equation 29 far from the origin. On the other hand, Theorem 1.2 uses Equation 29 for points near the origin as well. (ii) A picture like Figure 6.1 also appears in [K], though the purpose there seems somewhat different.

6.2 Four Dimensional Compactificaton

Here we take a close look at the mape E_j used in Equation 29.

Let $T_8^4 = (\mathbf{R}/8\mathbf{Z})^4$. Let

$$\delta_8(x) = 8\delta(x/8) \in \mathbf{R}/(8\mathbf{Z}). \quad (30)$$

Here $\delta(x)$ is the decimal part of x . Thus $\delta_8(x)$ computes $x \bmod 8\mathbf{Z}$. Consider the following embedding of \mathbf{R}^2 into T_8^4 :

$$\tilde{\psi}(x, y) = \left(\delta_8(x + y), \delta_8(x - y), \delta_8\left(\frac{x + y}{\phi}\right), \delta_8\left(\frac{x - y}{\phi}\right) \right). \quad (31)$$

We say that a strip map E , with associated triple (a_1, a_2, a_3) and vector $V = (v_1, v_2)$, is *special* if

- $a_1, a_2, a_3 \in \frac{1}{4}\mathbf{Z}[\phi]$ and $(a_1 + a_2) \in \frac{1}{2}\mathbf{Z}[\phi]$.
- $v_1, v_2 \in 2\mathbf{Z}[\phi]$ and $v_1 + v_2 \in 4\mathbf{Z}[\phi]$.

The triples associated to the strip maps E_1, \dots, E_4 from Equation 29 are:

$$\begin{array}{ll} \alpha_1 = (-1/4, +1/4, +3/4) & V_1 = (0, 4) \\ \alpha_2 = (-\phi/4, +1/2 - \phi/4, +1/2 - \phi/4) & V_2 = (-2, +2) \\ \alpha_3 = (-\phi/4, -1/2 - \phi/4, +1/2 - \phi/4) & V_3 = (+4 - 4\phi, 0). \\ \alpha_4 = (-1/4, -1/4, +3/4) & V_4 = (-2, -2). \end{array} \quad \text{Each of these}$$

triples is special.

The next lemma shows theoretically the maps E_1, \dots, E_4 have certain extensions $\tilde{E}_1, \dots, \tilde{E}_4$ defined on (most of) T_8^4 . In §7.8 we give the explicit formulas for $\tilde{E}_1, \dots, \tilde{E}_j$. The reader uninterested in the next lemma might try just to verify analytically that these formulas are correct. Our interest in the next lemma is that it allows us to *deduce* the formulas listed in §7.8 from a finite number of calculations, rather than having to verify them analytically.

Lemma 6.2 (Piecewise Affine Extension) *Let E be a special edge map. There is a finite union Y of flat 3-dimensional tori in T_8^4 together with a map $\tilde{E} : T_8^4 - Y \rightarrow T_8^4$ such that $\tilde{\psi} \circ E = \tilde{E} \circ \tilde{\psi}$ whenever both maps are defined. \tilde{E} is locally affine on each component of $T_8^4 - Y$ and the linear part of \tilde{E} is independent of component.*

Proof: Let $p_1 = (x_1, y_1)$ and $p_2 = (x_2, y_2)$, both points in \mathbf{R}^2 . Let f be the functional associated to E . Since $\mathbf{Z}[\phi] = \mathbf{Z}[\phi^{-1}]$ we can write

$$a_1 = \frac{1}{4}s_1 + \frac{1}{4\phi}t_1; \quad a_2 = \frac{1}{4}s_2 + \frac{1}{4\phi}t_2; \quad s_1, t_1, s_2, t_2 \in \mathbf{Z}; \quad s_j + t_j \in 2\mathbf{Z}.$$

This gives us

$$\begin{aligned} f(p_2) - f(p_1) &= \left(s_1 \frac{x}{4} + s_2 \frac{y}{4} \right) + \left(t_1 \frac{x}{4\phi} + t_2 \frac{y}{4\phi} \right) = \\ &= 2s_3 \left(\frac{x+y}{8} \right) + 2s_4 \left(\frac{x-y}{8} \right) + 2t_3 \left(\frac{x+y}{8\phi} \right) + 2t_4 \left(\frac{x-y}{8\phi} \right). \end{aligned} \quad (32)$$

Here $s_3, s_4, t_3, t_4 \in \mathbf{Z}$ are short linear combinations of s_1, s_2, t_1, t_2 . Hence

$$\delta(f(p_2) - f(p_1)) \leq CD(p_1, p_2) \quad (33)$$

for some constant C depending only on s_1, s_2, t_1, t_2 . Here D denotes Euclidean distance in T_8^4 . If $D(p_1, p_2)$ is sufficiently small then $f(p_2)$ lies closer to $f(p_1)$ than either number lies to \mathbf{Z} . Hence $\delta(f(p_2))$ is nonzero and E is defined on p_2 . Henceforth we assume this.

Define

$$N_j = -\text{floor}(f(p_j)). \quad (34)$$

If $D(p_1, p_2)$ is small enough then $N_2 - N_1$ is the integer closest to $f(p_2) - f(p_1)$. We can see directly from Equation 32 that $N_2 - N_1 = 2K$ with $K \in \mathbf{Z}$.

Recall that $V = (v_1, v_2)$ is the vector defining the edge map E . We have

$$E(p_2) - E(p_1) = (p_2 - p_1) + 2KV. \quad (35)$$

Here $E(p_1)$ is just some fixed value. To show that E , acting on T_8^4 , has a locally affine extension in a neighborhood of p_1 , it suffices to show that the coordinates of $\tilde{\psi}(2VK)$ are locally linear in the coordinates of $\tilde{\psi}(p)$. All these points are near 0 in T_8^4 , so we can just treat them as points in \mathbf{R}^4 . Let $(x', y') = 2KV$. We will show that $\delta_8(x' + y')$ is a linear function of the coordinates of $\tilde{\psi}(p)$. The other coordinates are done similarly.

We have

$$v_1 + v_2 = 4m + 4n\phi; \quad m, n \in \mathbf{Z}.$$

Hence

$$\delta_8(x' + y') = 8\delta\left(\frac{x' + y'}{8}\right) = 8\delta(mK + nK\phi) = 8\delta(nK\phi). \quad (36)$$

Since n is a uniformly bounded quantity, it suffices to show that $\delta(K\phi) \rightarrow 0$ as $D(p_1, p_2) \rightarrow 0$, and that $\delta(K\phi)$ is a linear combination of the coordinates of $\tilde{\psi}(p)$.

Define

$$\beta = s_3 \left(\frac{x+y}{8} \right) + s_4 \left(\frac{x-y}{8} \right) + t_3 \left(\frac{x+y}{8\phi} \right) + t_4 \left(\frac{x-y}{8\phi} \right);$$

Then $\delta(\beta) \rightarrow 0$ as $D(p_1, p_2) \rightarrow 0$.

Using the relation $\phi = 1 + \phi^{-1}$, we have

$$\phi\beta = s_5 \left(\frac{x+y}{8} \right) + s_6 \left(\frac{x-y}{8} \right) + t_5 \left(\frac{x+y}{8\phi} \right) + t_6 \left(\frac{x-y}{8\phi} \right);$$

where $s_5, s_6, t_5, t_6 \in \mathbf{Z}$ are integer linear combinations of s_3, s_4, t_3, t_4 . From this last equation we can see that Hence $\delta(\phi\beta) \rightarrow 0$ as $D(p_1, p_2) \rightarrow 0$. But then $\delta(K\phi) \rightarrow 0$ as well. Indeed,

$$K\phi = \beta\phi - \phi\delta(\beta) = \phi\beta = s_7 \left(\frac{x+y}{8} \right) + s_8 \left(\frac{x-y}{8} \right) + t_7 \left(\frac{x+y}{8\phi} \right) + t_8 \left(\frac{x-y}{8\phi} \right).$$

Since all the terms involving x and y are near integers, we have

$$\delta(K\phi) = s_7\delta\left(\frac{x+y}{8}\right) + s_8\delta\left(\frac{x-y}{8}\right) + t_7\delta\left(\frac{x+y}{8\phi}\right) + t_8\delta\left(\frac{x-y}{8\phi}\right). \quad (37)$$

This is what we wanted to prove.

The map E is defined on the complement of an infinite union of evenly spaced lines in \mathbf{R}^2 . These lines consist of points (x, y) such that

$$s_1 \frac{x}{4} + s_2 \frac{y}{4} + t_1 \frac{x}{4\phi} + t_2 \frac{y}{4\phi} \in \mathbf{Z}.$$

$\tilde{\psi}$ maps the union of these to a set that is dense in a finite union of flat 3 dimensional tori in T_8^4 . These flat tori have the following explicit description: Let Π be the family of 3-dimensional planes in \mathbf{R}^4 satisfying

$$s_1x_1 + s_2x_2 + t_1x_3 + t_2x_4 \in \mathbf{Z}.$$

Y is the image of Π in T_8^4 under the map

$$(x_1, x_2, x_3, x_4) \rightarrow (4(x_1 + x_2), 4(x_1 - x_2), 4(x_3 + x_4), 4(x_4 - x_4)) \pmod{8\mathbf{Z}}.$$

This completes our proof. ♠

6.3 Geometry of the Return Map

We begin with a consequence of the Pinwheel Lemma.

Lemma 6.3 *The map $\pi_1(\Upsilon_R(x, 1)) - (x, 1)$ only takes on finitely many values.*

Proof: To see this note that the “octagonal spiral” Σ in Figure 6.1 connecting the points $x_0, \dots, x_8, \zeta(x_8)$ is within a bounded distance of being symmetric about the origin. In other words, the image of Σ under reflection through the origin lies within a uniformly bounded tubular neighborhood of Σ . In terms of the displacement vectors $x_1 - x_0, x_2 - x_1, \dots$, we see that the opposite sides of Σ cancel up to a uniformly bounded error. Hence there are uniformly bounded integers α_j , depending on $(x, 1)$, such that $\Upsilon_R(x, 1) - (x, 1) = \sum \alpha_j V_j$. This establishes our claim. ♠

Now we return to the theme taken up in the Affine Extension Lemma. The analog of the Affine Extension Lemma is not quite true for the map ζ in Equation 29 but nonetheless a similar result holds. The domain for ζ is the union L of horizontal lines whose y -coordinates are odd integers. We really think of ζ as the union of two maps, ζ_+ and ζ_- , where $\zeta_+ : L_+ \rightarrow \mathcal{C}(+)$. here L_+ consists of those lines whose y -coordinates have the form $4k + 1$. The map ζ_- has a similar description. In this section we will treat ζ_+ , with the understanding that ζ_- has a similar treatment.

Consider the map $\psi : \mathcal{C}(\pm) \rightarrow \mathbf{T}^2$ given by

$$\psi(x, \pm 1) = [(x/(2\phi), x/2)] \quad (38)$$

Lemma 6.4 *There is an affine map $\tilde{\zeta} : T_8^4 \rightarrow \mathbf{T}^2$ such that $\tilde{\zeta} \circ \tilde{\psi} = \psi \circ \zeta$.*

Proof: We define

$$\tilde{\zeta}(x_1, x_2, x_3, x_4) = \left(\delta\left(\frac{x_1 + x_2}{4}\right), \delta\left(\frac{x_3 + x_4}{4}\right) \right).$$

This map is first of all defined from \mathbf{R}^4 to \mathbf{T}^2 , and then it respects the quotient. We compute that directly that $\tilde{\zeta} \circ \tilde{\psi} = \psi \circ \zeta_+$. ♠

Let

$$\tilde{T}^2(\pm) = \text{closure}(\tilde{\psi}(\mathcal{C}(\pm))) \subset T_8^4. \quad (39)$$

Notice that the first and third (or second and fourth) coordinates of $\tilde{\psi}$ completely determine the whole image of $\mathcal{C}(+)$ in T_8^4 . Thus $\tilde{T}^2(+)$ is a flat 2-dimensional torus. The same goes for $\tilde{T}^2(-)$.

Let \tilde{E}_j be the extension to T_8^4 of E_j . We give the explicit formula in §7.8. We define

$$\tilde{\Upsilon}_R : \tilde{T}^2(+) \rightarrow \mathbf{T}^2; \quad \tilde{\Upsilon}_R = \tilde{\zeta} \circ (\tilde{E}_4 \circ \dots \circ \tilde{E}_1)^2. \quad (40)$$

Combining the Piecewise Affine Extension Lemma with Lemma 6.4 we have

$$\tilde{\Upsilon}_R \circ \tilde{\psi} = \psi \circ \Upsilon_R \quad (41)$$

on $\mathcal{C}(\pm)$.

Lemma 6.5 (Constancy Lemma) *Suppose that $X \subset \tilde{T}^2(+)$ is a path connected open set on which the map Υ_R is entirely defined. Suppose that $(x_1, 1)$ and $(x_2, 1)$ are points of $\mathcal{C}(+)$ such that $\tilde{\psi}(x_j, 1) \in X$ for $j = 1, 2$. Then*

$$\pi_1(\Upsilon_R(x_1, 1)) - x_1 = \pi_1(\Upsilon_R(x_2, 1)) - x_2.$$

Proof: Since Υ_R is entirely defined on X it is also continuous on X . Consider the map

$$v(p) = \tilde{\Upsilon}_R(p) - \tilde{\zeta}(p)$$

This map is continuous on X .

A dense subset of X has the form $\tilde{\psi}(y, 1)$, where $y \in \mathcal{C}(+)$. For such points we have

$$\begin{aligned} v(\tilde{\psi}(y, 1)) &=^1 \tilde{\Upsilon}_R \circ \tilde{\psi}(y, 1) - \tilde{\zeta} \circ \tilde{\psi}(y, 1) =^2 \psi \circ \Upsilon_R(y, 1) - \psi \circ \zeta(y, 1) =^3 \\ &\psi \circ \Upsilon_R(y, 1) - \psi(y, 1) =^4 \psi(\pi_1(\Upsilon_R(y, 1)) - y, 1) \end{aligned} \quad (42)$$

The first equality is by definition; the second one is Equation 41 and Lemma 6.4; the third one is the fact that ζ is the identity on $\mathcal{C}(\pm)$; the fourth one comes from linearity, and from the fact that ψ only depends on the first coordinate. By Lemma 6.3, the map $\pi_1(\Upsilon_R(y, 1)) - y$ only takes on finitely many values. Therefore, $v(y, 1)$ takes on only finitely many values.

Now we know that the continuous map v only takes finitely many values on a dense subset of the path connected subset X . Therefore v is constant on X . Since v is constant on X we the calculation in Equation 42 is gives the same answer for all $y \in \mathcal{C}(+)$ such that $\tilde{\psi}(y) \in X$. The conclusion of the lemma follows immediately from setting $y = x_1$ and $y = x_2$. ♠

6.4 The Proof modulo a Computation

Recall that $\Psi : \mathbf{Z}^2 \rightarrow \mathbf{T}^2$ is our main map in the Arithmetic Graph Lemma. Recall that $T : \mathbf{Z}^2 \rightarrow \mathbf{R}^+$. If we identify \mathbf{R}^+ with either $\mathcal{C}(+)$ or $\mathcal{C}(-)$ then we have $\Psi = \psi \circ T$. Given a point $x_+ \in \mathcal{C}(+)$, let x_- be the point in $\mathcal{C}(-)$ with the same first coordinate. Let

$$v(x_{\pm}) = \pi_1(\Upsilon_R(x_{\pm}) - x_{\pm}). \quad (43)$$

Here is an essentially equivalent formulation of the Arithmetic Graph Lemma:

Lemma 6.6 *The points $\psi(x_+)$ and $\psi(x_-)$ always lie in one of the open polygons of the partition \mathcal{P} of \mathbf{T}^2 , and this polygon determines the unordered pair $\{v(x_+), v(x_-)\}$.*

What makes Lemma 6.6 equivalent to the Arithmetic Graph Lemma is that we do a finite amount of computation—all we need is one point per polygon—to check that the quantities given in Lemma 6.6, when hit with the map T^{-1} , match the types shown in Figure 2.5. We made millions of calculations to this effect. So, together with a small amount of computation, Lemma 6.6 implies the Arithmetic Graph Lemma.

The polygons of \mathcal{P} do not quite determine the *ordered* pair of numbers in Lemma 6.6. For this we need to pass to a finite cover. The map $\tilde{\zeta} : T_8^4 \rightarrow \mathbf{T}^2$ from Lemma 6.4 gives a finite covering map from $\tilde{T}^2(+)$ to \mathcal{T} . We lift the partition \mathcal{P} to a finite partition $\tilde{\mathcal{P}}$ of $\tilde{T}_2(+)$. We do the same thing for $\tilde{T}_2(-)$. Here is a reformulation of Lemma 6.6.

Lemma 6.7 *The point $\tilde{\psi}(x_+)$ lies in a polygon of $\tilde{\mathcal{P}}$ and this polygon determines $v(x_+)$. Likewise for $v(x_-)$.*

Again, we need a small amount of computation, one point per polygon of the partition, to verify that Lemma 6.7 is equivalent to Lemma 6.6 and the Arithmetic Graph Lemma.

Below we will prove

Lemma 6.8 *$\tilde{\Upsilon}_R$ is defined on each polygon of the partition $\tilde{\mathcal{P}}$ of $\tilde{T}^2(\pm)$.*

It follows immediately from Lemma 6.8 and from the Constancy Lemma that if $\tilde{\psi}(x_+)$ lies in a polygon of $\tilde{\mathcal{P}}$, then $v(x_+)$ is determined by this polygon.

Likewise for x_- . It only remains to show that $\tilde{\psi}(x_+)$ and $\tilde{\psi}(x_-)$ lie in the interior of a polygon of $\tilde{\mathcal{P}}$.

Suppose that this property fails. Then by symmetry both $\tilde{\psi}(x_+)$ and $\tilde{\psi}(x_-)$ lie in the boundary of some tile of $\tilde{\mathcal{P}}$, one on $\tilde{T}^2(+)$ and one on $\tilde{T}^2(-)$. But then $\tilde{\Upsilon}_R$ would be defined and continuous in a neighborhood of $\tilde{\psi}(x_+)$ on $\tilde{T}^2(+)$. But then two adjacent tiles of \tilde{P} on $\tilde{T}^2(+)$ would determine the same v values. The same goes for $\tilde{T}^2(-)$. But then two adjacent tiles of P would determine the same unordered pair of v values. We check computationally that this does not happen. Hence $\tilde{\psi}(x_+)$ and $\tilde{\psi}(x_-)$ always land in some tile of \tilde{P} . This verifies the hypotheses of Lemma 6.7.

6.5 Proof of Lemma 6.8

At this point we have reduced the Arithmetic Graph Lemma to Lemma 6.8. In this section we will prove Lemma 6.8 computationally.

We know that $\tilde{E}_{j+4} = \tilde{E}_j$ for $j = 1, 2, 3, 4$, but for notational purposes, it is convenient to forget this fact and just consider $\tilde{E}_1, \dots, \tilde{E}_8$. We let

$$\tilde{F}_k = \tilde{E}_k \dots \tilde{E}_1. \quad (44)$$

We interpret \tilde{F}_0 as the identity map. Also, $\tilde{\Upsilon}_R = \tilde{\zeta} \circ \tilde{F}_8$. To show that $\tilde{\Upsilon}_R$ is defined at some point x it suffices to show that the maps $\tilde{F}_1, \dots, \tilde{F}_8$ are all defined on x .

We will see from the explicit description of our map \tilde{E}_k , given in §7.8, that there is a union Y_k of two 3-tori, such that $T_8^4 - Y_k$ consists of two connected components $C_k(0)$ and $C_k(1)$ on which the map \tilde{E}_k is entirely defined and locally affine.

If $\tilde{\Upsilon}_R$ is defined on a point $x \in T_8^4$ then we can define a length 8 binary sequence $\epsilon_1, \dots, \epsilon_8$, by the property that $\tilde{F}_{k-1}(x) \in C_k(\epsilon_k)$ for $k = 1, \dots, 8$. In short, we can associate a canonical binary sequence of length 8 to any point x on which $\tilde{\Upsilon}_R$ is defined. We call this sequence the *itinerary* of x .

Here we define a slightly more general notion of an itinerary. Given an itinerary $\epsilon_1, \dots, \epsilon_8$ we can define \tilde{E}_k on Y by demanding that \tilde{E}_k extends continuously to the closure of $C_k(\epsilon_k)$. Then \tilde{E}_k is completely defined on T_8^4 . It is continuous on the closure of $C_k(\epsilon_k)$ and on the interior of $C_k(1 - \epsilon_k)$, but not globally continuous. With this definition, we say that $x \in T_8^4$ has *extended itinerary* $\epsilon_1, \dots, \epsilon_8$ if the maps \tilde{F}_k (when extended) are all defined on x and $\tilde{F}_{k-1}(x)$ lies in the closure of $C_k(\epsilon_k)$ for $k = 1, \dots, 8$. Put another way,

x has extended itinerary ϵ provided there exist points arbitrarily close to x that have itinerary ϵ .

We define the *stretch* of a convex polygon P to be the maximum distance in T_8^4 between consecutive vertices of P . We denote this by $\sigma(P)$.

Lemma 6.9 (Definedness Criterion) *Suppose that*

- $\tilde{\Upsilon}_R$ is defined on some point of P , and this point has itinerary ϵ .
- All the vertices of P have extended itinerary ϵ .
- The stretch of $\tilde{F}_k(P)$ is less than $2\sqrt{2}$ for each $k = 0, \dots, 7$.

Then $\tilde{\Upsilon}_R$ is defined on all points of R , and all these points have itinerary ϵ .

Proof: Looking at the nature of our determiner functions d_k , we see that the Euclidean distance between separate components of Y_k is at least $2\sqrt{2}$. Hence, if v_1, v_2 are two points in the closure of $C_k(\epsilon_k)$ which are less than $2\sqrt{2}$ apart, then either the line segment $\overline{v_1v_2}$ lies in the closure $\overline{C}_k(\epsilon_k)$.

Suppose we have shown by induction that \tilde{F}_{k-1} is defined on P . Let $P' = \tilde{F}_{k-1}(P)$. The hypotheses of this lemma say that every edge of P' has length less than $2\sqrt{2}$, and the endpoints of such an edge are in $\overline{C}_k(\epsilon_k)$. Hence, all the edges of P' lie in $\overline{C}_k(\epsilon_k)$. Since $\partial C_k(\epsilon_k)$ is three dimensional, and (by induction) P' is a planar polygon, we must have $P' \subset \overline{C}_k(\epsilon_k)$.

If some point of the open P' actually lies in $\partial C_k(\epsilon_k)$ then all of P' must lie in $\partial C_k(\epsilon_k)$. The point here is that the tangent plane at this bad point must be contained in the tangent space to Y_k , because there is no crossing allowed. We also know that some point of P' lies in $C_k(\epsilon_k)$, so the above bad situation cannot occur. Hence all points of P' lie in $C_k(\epsilon_k)$. This completes the induction step. ♠

We now mention a trick that makes the Definedness Criterion more useful. Given a line segment $s \in T_8^4$, with endpoints p_1 and p_2 , we let s' denote the partition of s into the two segments $[p_1, q]$ and $[q, p_2]$ where

$$q = p_1\phi^{-2} + q_2\phi^{-1}. \tag{45}$$

Note that $q \in s$ because $\phi^{-1} + \phi^{-2} = 1$. We might have chosen q to be the midpoint of s , but our choice interacts better with $\mathbf{Z}[\phi]$. Given a polygon

P , we let P' denote the polygon, with twice as many vertices, obtained by subdividing each edge of P . In general, let $P^{(n)} = (P^{(n-1)})'$. Then $P^{(n)}$ has 2^n times as many vertices as P and the stretch of $P^{(n)}$ is ϕ^{-n} times the stretch of P . Thus, by taking a sufficiently large integer n , we can guarantee the last condition of the Discreteness Criterion without even computing the stretch.

We take each polygon P of our partition $\tilde{\mathcal{P}}$ and perform the following calculation. We take the 10th subdivision $P^{(10)}$ and check the Definedness Criterion. (This is overkill.) This verifies Lemma 6.8. We give details of the calculation in §7.8.

7 The Code in Detail

7.1 Arithmetic Operations

We do all our computations with complex numbers of the form

$$\frac{x_0 + x_1\phi}{2} + I \frac{x_2 + x_3\phi}{2}. \quad (46)$$

We call such a number an `IntegerComplex` and represent it as a sequence

$$\{x_0, x_1, x_2, x_3\}. \quad (47)$$

Given a and b , both `IntegerComplex` objects, we perform the following operations:

- $a + b$ and $a - b$ are computed by adding or subtracting components.
- $2ab$, another `IntegerComplex`, is computed by expanding out all the terms and grouping them.
- The conjugate \bar{a} is obtained by negating the third and fourth coordinates of a .
- We have a routine `interpolate(a,b)`, which computes $a\phi^{-1} + b\phi^{-2} \in [a, b]$.

Now we explain how we test the sign of the number $a = a_0 + a_1\phi$. Since ϕ is irrational, we need a trick. The idea is to consider

$$f_{50} = 12586269025; \quad f_{51} = 20365011074 \quad f_{52} = 32951280099. \quad (48)$$

Here f_n is the n th Fibonacci number. The quantity $a_0 + a_1\phi$ is positive (respectively negative) provided that both sums

$$s_1(a) = a_0f_{50} + a_1f_{51}; \quad s_2(a) = a_1f_{51} + a_2f_{52} \quad (49)$$

are positive (respectively negative). This works because the sign of the difference $\phi - f_{n+1}/f_n$ alternates with n . The routine `sign` below never fails for our computations. We implement `sign` using the `BigInteger` class in Java, which does integer arithmetic correctly on huge integers.

```

sign( $a$ ):
if( $a_0 = 0$  and  $a_1 = 0$ ) return(0)
if( $s_1(a) > 0$  and ( $s_2(a) > 0$ ) then return(1).
if( $s_1(a) < 0$  and ( $s_2(a) < 0$ ) then return(-1).
otherwise fail

```

We take the decimal part of a `IntegerComplex` using floating point arithmetic to compute the nearest integer. The computation of n does not use exact integer arithmetic, but then we use the `sign` routine to check rigorously that our guess always lies in $[-1/2, 1/2]$. Here is the routine:

```

dec( $a, b$ ):
Let  $n$  be the integer nearest  $(a + b\phi)/2$ , evaluated as a double.
Check that  $(a - 2n, b)$  lies in  $[-1/2, 1/2]$  using sign.
if this is true, then return( $a - 2n, b$ ). Otherwise fail.

```

Here we explain the `IntegerComplex` version of our map Ψ given in Equation 7.

```

psi( $a, b$ ):
let  $x = 4 - 12a + 4b$  and  $y = 8a - 2$ . (the IntegerComplex version of Eq 3)
Let  $c_1 = \{(-x + y)/2, x/2\}$ . (division by  $2\phi$ )
Let  $c_2 = \{x/2, y/2\}$ . (division by 2)
Let  $d_j = \mathbf{dec}(c_j)$  for  $j = 1, 2$ .
return( $d_1 + Id_2$ ).

```

Our division by 2ϕ and by 2 works because the integers x and y are both even. This, our routine really does return a `IntegerComplex`.

7.2 Classification into Types

An `IntegerPolygon` is a finite list of `IntegerComplex` objects. The complex numbers represented by the `IntegerComplex` objects are the vertices of a convex polygon. In this section we explain our routines which decide if an `IntegerComplex` is contained in an `IntegerPolygon`. Our test is based on a routine `signArea`, which uses the routine `sign` to compute the signed area of a triangle whose vertices are `IntegerComplex` objects.

Given an `IntegerComplex` z and an `IntegerPolygon` P , let $T_i(z, P)$ de-

note the triangle determined by the ordered triple of `IntegerComplex` objects z , $P(i)$ and $P(i + 1)$. The indices are taken cyclically. The following routine returns a 1 if z is contained in the interior of P and a 0 otherwise. A straightforward variant, `IsContainedClosed` checks if $z \in \overline{P}$.

```

isContainedOpen(z,P):
loop for the number of vertices of P:
  check that  $T_i(z, P)$  and  $T_{i+1}(z, P)$  have nonzero signArea
  if(false) return(0)
  check that  $T_i(z, P)$  and  $T_{i+1}(z, P)$  have the same signArea
  if(false) return(0)
endloop
return(1)

```

Recall that the arithmetic graph Γ is a certain subset of $\mathbf{Z}^2 \cap H$, where H is a certain half-plane. Each point $(x, y) \in \mathbf{Z}^2$ has a type, which we compute by determining which open polygon of \mathcal{P} contains $\Psi(x, y) \in T^2$. Here we explain how we compute this in practice. Lifting \mathcal{P} to \mathbf{R}^2 we get a tiling $\tilde{\mathcal{P}}$ of \mathbf{R}^2 . We compute the point `psi(x,y)` and check which tile of $\tilde{\mathcal{P}}$ it lands in. We have arranged that the image of `psi` is fairly close to the origin, and so we only have to check a smallish portion of the tiling.

We accomplish our goal using two routines. The first of our routines checks whether or not an `IntegerComplex` z near the origin in \mathbf{R}^2 is contained in a union of Λ -translates of a given `IntegerPolygon` P . The program returns a 1 if the answer is yes.

```

isLatticeContainedOpen(z,P):
loop over  $i$  from  $-3$  to  $3$  and over  $j$  from  $-3$  to  $3$ 
   $zz = \text{moveLattice}(z, i, j)$ 
  if(isContainedOpen( $zz, P$ ) = 1 then return(1)
endloop

```

We always take P as one of the polygons from our partition \mathcal{P} . These polygons are listed in §7.5. (See also Figure 2.5.) Our routine `classify` combines our routine `psi` with the routine `isLatticeContainedOpen` to classify each point of \mathbf{Z}^2 into the local types.

We use the routine `isContainedClosed` in place of `isContainedOpen` in case we want to check that a given point is contained in a closed polygon.

7.3 Types and Dynamical Translations

As we discussed in the previous section, there are 23 nontrivial local types of vertex in the arithmetic graph, as shown in Figure 2.4. We list these types here (rather than in the appendix.)

$$\begin{array}{cc} T_j & \\ a_1 & b_1 \\ a_2 & b_2 \end{array} \quad (50)$$

Indicates that one of the edges emanating from a vertex of type T_j . is (a_1, a_2) and the other one is (b_1, b_2) . In other words, the two columns of the matrix encode the type. The ordering of the two columns is arbitrary. We list the types T_1, T_3, \dots, T_{23} . Similar to what happens above, T_{2j} is obtained by negating all the entries of T_{2j-1} , for $j = 1, \dots, 11$. Here is the list:

$$\begin{array}{cccc} T_1 & T_3 & T_5 & T_7 \\ \begin{array}{cc} 1 & 0 \\ 1 & 1 \end{array} & \begin{array}{cc} -1 & 1 \\ 1 & 1 \end{array} & \begin{array}{cc} -1 & 0 \\ 1 & -1 \end{array} & \begin{array}{cc} -1 & 0 \\ 1 & -1 \end{array} \\ T_9 & T_{11} & T_{13} & T_{15} \\ \begin{array}{cc} 0 & -1 \\ 1 & -1 \end{array} & \begin{array}{cc} 1 & -1 \\ 1 & 0 \end{array} & \begin{array}{cc} 1 & -1 \\ 1 & 0 \end{array} & \begin{array}{cc} 0 & -1 \\ -1 & 0 \end{array} \\ T_{17} & T_{19} & T_{21} & T_{23} \\ \begin{array}{cc} 0 & -1 \\ -1 & 0 \end{array} & \begin{array}{cc} 0 & -1 \\ 1 & 0 \end{array} & \begin{array}{cc} 0 & 0 \\ 1 & -1 \end{array} & \begin{array}{cc} 0 & 0 \\ 1 & -1 \end{array} \end{array}$$

For each of these types, there are two associated dynamical translations of T^2 . Referring to the matrix in Equation 50, the two maps are:

$$(x, y) \rightarrow [(a_1\phi^{-4} + a_2\phi^{-1}, a_1\phi^{-3})]; \quad (x, y) \rightarrow [(b_1\phi^{-4} + b_2\phi^{-1}, b_1\phi^{-3})]. \quad (51)$$

These maps relate the points $\Psi(v)$ and $\Psi(v')$ where v is the vertex and v' is one of the vertices connected to v by the arithmetic graph. The following routine starts with a pair (x, y) obtained from one of the columns of the above matrices and returns the `IntegerComplex` z which effects the corresponding dynamical translation. That is, on \mathbf{R}^2 the dynamical translation is given by $w \rightarrow w + z$.

`getMap(x,y):`

return the integer complex with coordinates $(10x - 2y, -6x + 2y, -6x, 4x)$

7.4 The Sequence Generator

If v_1 and v_2 are two consecutive vertices of the arithmetic graph, then one of the two maps associated to v_1 coincides with one of the two maps associated to v_2 . For instance, if a vertex is type 1 is connected to a vertex of type 21 we could write

$$\begin{array}{ccc} T_1 & T_{21} & \\ 1 & 0 & 0 \\ 1 & 1 & -1 \end{array} \quad \text{or} \quad \begin{array}{cc} 1 & 21 \\ 1 & 0 \\ 1 & 1 \end{array}$$

The second notation system is a simplification of the first. We drop off the last column because it is not of interest to us. The information in the right hand side array is enough to generate both v_1 and v_2 and also to determine the type of v_1 .

More generally, given a point $p \in \Gamma$ and a choice $\epsilon \in \{1, 2\}$ and some positive integer k , there is an array

$$A(p, \epsilon, k) = \begin{array}{cccc} & a_1 & a_2 & \dots & a_k \\ x_1 & x_2 & \dots & x_k & \\ y_1 & y_2 & \dots & y_k & \end{array} \quad (52)$$

that contains the information needed to draw the k consecutive vertices $p = v_1, \dots, v_k$ of Γ heading in the direction determined by ϵ . The two arrays $A(p, 1, k)$ and $A(p, 2, k)$ determine the portion of Γ which starts at p and moves k units in either direction.

Choosing $k = 3$ and p to be one of the center points of a gene, the two 3×2 arrays encode the structure of that gene. Here is an example. Our first gene is located at the point $p = (3, 4)$. The two arrays are

$$A((3, 4), 1, 3) = \begin{array}{ccc} 11 & 9 & 23 \\ 1 & 0 & 0 \\ 1 & 1 & 1 \end{array} ; \quad A((3, 4), 2, 3) = \begin{array}{ccc} 11 & 14 & 10 \\ -1 & -1 & 0 \\ 0 & -1 & -1 \end{array}$$

This tells us that the 5 vertex types we see along the gene A_0 are (in one of the two orders) 10, 14, 11, 9, 23. Looking at the first column of $A((3, 4), 1, 3)$, we can see that that the vector $(1, 1)$ connects the point of type 11 to the point of type 9. In this way, we can draw a copy of the gene given the above arrays.

The next routine generates the arrays for the point $p = (x, y) \in \mathbf{Z}^2$.

`getOrbit(x,y,length,epsilon):`

1. let A be the empty array
2. let $X = x$ and $Y = y$. 3. let count= 0
4. while(count<length):
 - $a = \text{classify}(X, Y)$
 - Let M be the matrix associated to T_a
 - If(count= 0) then:
 - append to A the (epsilon)th column of M
 - if(count> 0) then:
 - append to A the col. of M which does not match the last col. of A .
 - Let m_x and m_y denote the entries of the column of M used above.
 - replace X by $X + m_x$
 - replace Y by $Y + m_y$
 - increment count
5. return(A)

`getOrbit` runs until the count equals the length, and then breaks. At that point, the array A is returned. For our purposes, we need to get both sequences associated to p and k . So, we run the above routine once for $\epsilon = 1$ and once for $\epsilon = 2$. We call the resulting pair (L, R) of arrays the *k-itinerary* of $p \in \mathbf{Z}^2$.

To deal with the genes, we are interested in the case $k = 3$. However, the reader can draw a large portion of Γ_0 by taking a large value of k and then reading off the segments of the strand from the resulting arrays.

7.5 Checking the Dynamical Polygons

Each array A as in Equation 52 determines a dynamical polygon $Y = Y(A)$, as in §4.2. Here we explain how to check directly that a point $s \in T^2$ lies in the closure of Y or else in the interior of Y (depending on our interest.) The point s is always given as the projection to T^2 of a certain lift $s \in \mathbf{R}^2$ which we give the same name. Let $P(j)$ denote the j th tile in the partition \mathcal{P} of T^2 . As above, we identify $P(j)$ with a particular lift to \mathbf{R}^2 . The following routine returns a 1 provided that s is contained in the interior of Y .

```

matchOrbitOpen(s,A):
let  $S = s$ 
loop for  $i = 1$  to length of  $A$ 
  check that isLatticeContainedOpen(S,P(ai))= 1.

```

```

if false return(0)
if true then:
  let  $z = \text{getMap}(x_i, y_i)$ 
  let  $S = S + z$  (act on  $S$  by the dynamical translation)
endloop

```

As a variant, we check that s is contained in the closure of Y by using `isLatticeContainedClosed` in place of `isLatticeContainedOpen`.

We can now explain exactly how we check our guess Y_G for the 75 dynamical polygons associated to the 75 genes. Here is the 3-step process.

- For the j th gene A_j we let (x_j, y_j) be the location of the center a_j of A_j . We use `getOrbit` (x_j, y_j) to generate the 3-itinerary $A = (L_j, R_j)$.
- We check that each `IntegerComplex` v representing a vertex of Y_G is contained in the closure of $Y = Y_A$ using `matchOrbitClosed` (v, L_j) and then `matchOrbitClosed` (v, R_j) .
- For each edge e of Y_G we produce a `IntegerComplex` v contained in the interior of e by applying `interpolate` to the two endpoints of e . Given v we then check that one of the two runs `matchOrbitOpen` (v, L_j) and `matchOrbitOpen` (v, R_j) returns a 0. This is to say that v is not contained in the interior of Y .

We list the dynamical polygons Y_0, \dots, Y_{74} in §8.2. We list the centers for our genes in §8.3.

7.6 The Shadowing Property

We begin by recalling the basic setup. Let A be a gene from our inflation generator and let B be the gene core. Let a be the center vertex of A . Let A' be the strand which shadows $D(A)$. Let Y be the dynamical polygon associated to A and let Y' be the dynamical polygon associated to A' . Let β be the inflation map and let $\gamma : Y \rightarrow T^2$ be the associated similarity. We want to verify that $\gamma(Y) \subset Y'$. There are two main steps to this verification:

1. Find the dynamical sequences (as in Equation 52) associated to A' ;
2. Compute γ .

Once we have completed these steps, we check that γ maps each vertex of Y into the closure of Y' . This shows that γ maps the interior of Y into the interior of Y' , which is what we want.

7.6.1 Finding the Dynamical Sequences

We store A' as a triple points

$$((x_1, y_1), (x_2, y_2), (x_3, y_3))$$

In §8.4 we give the list of triples. Here (x_2, y_2) is the point a' that comes close to $D(a)$, and (x_1, y_1) and (x_3, y_3) are the two endpoints of A' . First of all, we explain the routine that recovers the sequence of types (as in Equation 52 associated to A'). This routine is a variant of the routine `getOrbit`.

The routine `getOrbit` starts at the point a and moves k steps in either direction, using the dynamical translations to move the point $\Psi(p)$ around the partition \mathcal{P} . (We only care about the case $k = 3$.) Our new version does the same thing, with one twist: Rather than stopping after k steps, the routine stops when we reach either (x_1, y_1) or (x_3, y_3) . Referring to the routine `getOrbit` written above, we simply change the line

4. while(count<length):

to the line

4'. while(current point in \mathbf{Z}^2 does not equal (x_1, y_1) or (x_3, y_3)):

Technically we could avoid this reconstruction problem just by saving the sequences attached to A'_1, \dots, A'_{75} , but we prefer not to store so much data. Below we will list out the 75 triples.

7.6.2 Computing the similarity

We have already defined the routine `psi` above, which chooses some lift of $\Psi(a)$ to \mathbf{R}^2 . Here we explain an improved version, which chooses the lift of $\Psi(a)$ that is contained in Y . The idea is to find a “correction vector” λ in the lattice Λ such that `psi(a)+λ` $\in P$. The idea is simply to enumerate the short vectors $\lambda_1, \dots, \lambda_k \in \Lambda$ and check which ones work. For us, $k = 225$. Here is our routine:

```

canonicalPsi(k):
Let  $a = a_k$  the center point of  $A_k$ .
loop from  $i = -7$  to  $7$ 
  loop from  $j = -7$  to  $7$ 
    let  $\lambda = i(1, \phi^{-1}) + j(0, 1)$ .
    if  $\mathbf{psi} + \lambda \in Y_k$  then return  $\lambda$ 
  endloop
endloop
if no choice works then fail

```

The routine never fails when we run it for $j = 1, \dots, 75$. From the way we have constructed A' , we know that γ maps $\mathbf{canonicalPsi}(a)$ into Y' . Thus, we can use our knowledge of $\mathbf{canonicalPsi}(a)$ to compute γ . We seek a pair of integers (m, n) such that

$$\gamma = \gamma_0 + [(m\phi^{-4} + n\phi^{-1}, 0)]; \quad \gamma_0(x, y) = (-\phi^{-3}x, -\phi^{-3}y). \quad (53)$$

We set $y = \mathbf{canonicalPsi}(a)$ and then test small integer choices of m and n until we find a choice which leads to $\gamma(y) \in Y'$. To test that $\gamma(y) \in Y'$ we don't need to compute Y' . We simply check that $\gamma(y)$ follows the dynamical sequences associated to A' . In other words, we just go back to the definition of Y' . We make the same kind of loop as in the routine $\mathbf{canonicalPsi}$, with $|m|, |n| \leq 7$. This always works.

Once we have γ we list out the vertices of Y as Y_1, \dots, Y_k and check that $\gamma(Y_i)$ follows the dynamical sequences associated to Y' . Here $k \leq 5$ for each of the 75 choices.

7.7 Checking Coherence

Let g_1, \dots, g_{1024} be the first 1024 points along Γ_0 . We list the first few points below. The point g_j is the center of a gene G_j . Let β_j be the inflation map we associate to G_j using our inflation structure χ . The list $\beta_1, \dots, \beta_{1024}$ consists of multiple references to the same 75 inflation maps because each G_j has one of the 75 gene types. For each index j we produce a point $g'_j \in \Gamma_0$, always within 3 units of $D(g_j)$, such that

$$\Psi(g'_j) = \gamma \circ \Psi(g_j). \quad (54)$$

This is to say that $\beta_j(g_j) = g'_j$. We check visually that g'_1, \dots, g'_{1024} lie in order on Γ_0 . This verifies the coherence of our inflation generator.

Billiard King simply stores the 1024 points g'_1, \dots, g'_{1024} . We then run the following test.

verifyCoherence:

loop from $j = 1$ to 1024.

1. Let $k = I_j$ (the gene type of G_j)
2. let $y_j = \text{canonicalPsi}(g_j)$
3. let γ be the map computed in Equation 53 for the index k .
4. Check that $\gamma(y_j)$ and $\text{psi}(g_j)$ agree up to the lattice Λ .

endloop

In reference to line 4 above, the check amounts to exhibiting a short vector $\lambda \in \Lambda$ such that $\gamma(y_j) = \text{psi}(g_j) + \lambda$. We look at 225 vectors. In the interest of space we don't list the 1024 points in the appendix. Here is the routine that generates these points:

generateShadow(j):

1. Let $k = I_j \in \{1, \dots, 75\}$ be the type of the gene G_j
2. Let a_k be the center of the k th gene in our inflation generator
3. Let a'_k be the point of A'_k that shadows $D(a_k)$
4. Search for a point $g'_j \in \mathbf{Z}^2$ within 3 units of $D(g_j)$ such that g'_j and a'_k are the centers of equivalent genes.

Using the notation $g_j \longrightarrow g'_j$ we list the first 4 points.

$$(1, 1) \longrightarrow (3, 4) \quad (1, 2) \longrightarrow (3, 9) \quad (1, 3) \longrightarrow (3, 13) \quad (2, 4) \longrightarrow (8, 18).$$

7.8 Checking the Partition

Here we explain the calculations from the end of §6 that we make for our proof of the Arithmetic Graph Lemma. First of all, we list out explicit formulas for the maps $\tilde{E}_1, \dots, \tilde{E}_4$ from the Affine Extension Lemma. After we have these formulas, we explain the calculation.

7.8.1 Explicit Formulas

Let \tilde{E}_j be the extension of E_j to T_8^4 guaranteed by the Affine Extension Lemma. We can rigorously compute the formulas for these maps just by

making a few calculations. (We checked the formulas on millions of points.)

One general feature of the map \tilde{E}_j is that the corresponding “undefined set” Y_j consists of two parallel 3-tori. The complementary region $T_8^4 - Y_j$ consists of two regions. This feature is not necessarily clear from our description, because we describe our maps in terms of coordinates on the set $(-4, 4)^4$, which is the interior of a fundamental domain for T_8^4 . The action on T^4 is obtained by piecing together the definitions across the boundaries of $[-4, 4]^4$.

In all cases, we will list the following data:

- The linear map L .
- A *determiner function* $d : (-4, 4)^4 \rightarrow \mathbf{R}$.
- A partition of \mathbf{R} either into 3 or 5 intervals. In the 3-interval case, the dividing points are 0 and 4 and the intervals are $(-\infty, 0)$ and $(0, 4)$ and $(4, \infty)$. In the 5-interval case, the dividing points are $-8, -4, 0, 4$ and the intervals are determined similarly.
- For each interval I of the partition we give an array of the form

$$v(I) = \begin{bmatrix} a_{11} & a_{21} & a_{31} & a_{41} \\ a_{12} & a_{22} & a_{32} & a_{42} \end{bmatrix}$$

This array stands for the vector

$$\left(\frac{a_{11} + a_{12}\phi}{2}, \frac{a_{21} + a_{22}\phi}{2}, \frac{a_{31} + a_{32}\phi}{2}, \frac{a_{41} + a_{42}\phi}{2} \right)$$

In case all the entries of the array are 0 we will save space by just writing [0] in place of the array. Our map is then given by $\tilde{E}(x) = L(x) + v(I)$, where I is such that $d(x) \in I$. This definition makes sense except for the points x where $d(x)$ lies in one of the dividing points listed above.

$$\begin{aligned} \tilde{E}_1 : \quad L_1(x) &= \begin{pmatrix} x_1 \\ x_2 \\ x_2/\phi + x_3 + x_4 \\ x_2/\phi \end{pmatrix}; \quad d_1(x) = x_1 + 1; \\ & \begin{bmatrix} 1 & 1 & 1 & 1 \\ 0 & 0 & -1 & 1 \end{bmatrix}; \quad [0] \quad \begin{bmatrix} 1 & 1 & 1 & 1 \\ 0 & 0 & 1 & -1 \end{bmatrix}. \end{aligned} \tag{55}$$

$$\begin{aligned}
\tilde{E}_2 : \quad L_2(x) &= \begin{pmatrix} x_1 \\ x_2 \\ x_3 \\ -x_1 + x_2/\phi + x_3\phi \end{pmatrix}; \quad d_2(x) = x_2 + x_3 - \frac{1}{\phi^2}; \\
\begin{bmatrix} 0 & 0 & 0 & 0 \\ 0 & 0 & 0 & 2 \end{bmatrix} & \begin{bmatrix} 0 & 1 & 0 & 1 \\ 0 & 0 & 0 & 1 \end{bmatrix} \quad [0] \quad \begin{bmatrix} 0 & 1 & 0 & 1 \\ 0 & 0 & 0 & -1 \end{bmatrix} \quad \begin{bmatrix} 0 & 0 & 0 & 0 \\ 0 & 0 & 0 & -2 \end{bmatrix} \quad (56)
\end{aligned}$$

$$\begin{aligned}
\tilde{E}_3 : \quad L_3(x) &= \begin{pmatrix} x_1\phi - x_2 - x_3 + x_4\phi \\ x_1/\phi - x_3 + x_4\phi \\ -x_1/\phi + x_2 + 2x_3 - x_4\phi \\ -x_1/\phi + x_2 + x_3 - x_4/\phi \end{pmatrix}; \quad d_3(x) = x_1 + x_4 - \frac{1}{\phi^2}; \\
\begin{bmatrix} 0 & 0 & 0 & 0 \\ 2 & 2 & -2 & -2 \end{bmatrix} & \begin{bmatrix} 1 & 1 & 0 & 0 \\ 1 & 1 & -1 & -1 \end{bmatrix} \quad [0] \quad \begin{bmatrix} 1 & 1 & 0 & 0 \\ -1 & -1 & 1 & 1 \end{bmatrix} \quad \begin{bmatrix} 0 & 0 & 0 & 0 \\ -2 & -2 & 2 & 2 \end{bmatrix} \quad (57)
\end{aligned}$$

$$\begin{aligned}
\tilde{E}_4 : \quad L_4(x) &= \begin{pmatrix} x_1 \\ x_2 \\ x_1/\phi \\ x_4 \end{pmatrix}; \quad d_4(x) = x_0 + 1 \\
\begin{bmatrix} 1 & 0 & 1 & 0 \\ 0 & 0 & 1 & 0 \end{bmatrix} & \quad [0] \quad \begin{bmatrix} 1 & 0 & 1 & 0 \\ 0 & 0 & -1 & 0 \end{bmatrix}. \quad (58)
\end{aligned}$$

7.8.2 Reducing to Planar Polygons

The polygons in the partition $\tilde{\mathcal{P}}$ are subsets of the torus $T_{\mathfrak{s}}^4$. In this section we explain how we arrange our computation so that we just have to consider polygons which are subsets of \mathbf{R}^4 .

Let

$$T_4^2 = \mathbf{R}^2 / (4\mathbf{Z}^2).$$

Then T_4^2 is a square torus which is naturally a 16-fold cover of \mathbf{T}^2 . Let $\hat{\mathcal{P}}$ denote the lift of \mathcal{P} to T_4^2 . If P_k is a polygon of \mathcal{P} , then P_k is the projection

to \mathbf{T}^2 of the convex hull of certain vertices $\{v_{k1}, \dots, v_{kn}\}$. For each $(\epsilon_1, \epsilon_2) \in \{0, 1, 2, 3\}^2$ we can form the convex polygon $P_k(\epsilon_1, \epsilon_2)$ with vertex list

$$\{v_{k1} + (\epsilon_1, \epsilon_2), \dots, v_{kn} + (\epsilon_1, \epsilon_2)\} \quad (59)$$

and project it into T_4^2 . Call the resulting polygon $\widehat{P}_k(\epsilon_1, \epsilon_2)$. The union of the polygons $\widehat{P}_k(\epsilon_1, \epsilon_2)$, taken over all indices, gives us the partition $\widehat{\mathcal{P}}$. So, just to be clear, $P_k(\epsilon_1, \epsilon_2)$ is some concrete lift to R^2 of a polygon of the partition $\widehat{\mathcal{P}}$.

We are interested in the polygons of the partition $\widetilde{\mathcal{P}}$, which is a subset of the different torus T_8^4 . We now explain how to translate between $\widehat{\mathcal{P}}$ and $\widetilde{\mathcal{P}}$. We introduce the maps μ_- and μ_+ , defined by

$$\mu_-(x, y) = ((\delta_8(2x + 1), \delta_8(2x - 1), \delta_8(2y + \phi^{-1}), \delta_8(2y - \phi^{-1})))$$

$$\mu_+(x, y) = ((\delta_8(2x - 1), \delta_8(2x + 1), \delta_8(2y - \phi^{-1}), \delta_8(2y + \phi^{-1})))$$

We also introduce the map

$$\widehat{\psi}(x) = (\delta_4(x/(2\phi)), \delta_4(x/2)) = (4\delta(x/(8\phi)), 4\delta(x/8)) \in T_4^2. \quad (60)$$

We compute that

$$\mu_+ \circ \widehat{\psi}(x, 1) = \widetilde{\psi}(x, 1); \quad \mu_- \circ \widehat{\psi}(x, -1) = \widetilde{\psi}(x, -1).$$

It follows from this last equation that μ_+ maps the polygons of $\widehat{\mathcal{P}}$ to the polygons of $\widetilde{\mathcal{P}}$ which partition $\widetilde{T}^2(+)$. A similar statement holds for μ_- .

We can think of μ_+ and μ_- as being defined on \mathbf{R}^2 , and thus the polygons of $\widetilde{\mathcal{P}}$ all have the form

$$\mu_{\pm}(P_k(\epsilon_1, \epsilon_2))$$

for $k = 1, \dots, 26$ and $\epsilon_j \in \{0, 1, 2, 3\}$.

7.8.3 The Calculation

We use the same arithmetic as described above to do the calculations from §6. First we define a routine that produces a lift of the a_2 nd point of $\mu_{\pm}(Q)$, where $Q = Q_{a_1}(a_3, a_4)$. The integer $a_5 \in \{0, 1\}$ determines whether we take μ_+ or μ_- . Here is the routine.

`getVertexPlanar(a_1, a_2, a_3, a_4, a_5):`

Let $v = x_0 + iy_0$ be the a_2 vertex of our particular lift of P_{a_1} .

Let $x_2 = x_1 + a_3$ and $y_2 = y_1 + a_4$. (Equation 59.)

If $a_5 = 0$ then return $(2x_1 + 1, 2x_2 - 1, 2y_2 + 1/\phi, 2y_2 - 1/\phi)$. (apply μ_+ .)

If $a_5 = 1$ then return $(2x_1 - 1, 2x_2 + 1, 2y_2 - 1/\phi, 2y_2 + 1/\phi)$. (apply μ_- .)

Next, we have a routine **dec8**, which computes $x \bmod 8\mathbf{Z}$, where $x \in \frac{1}{2}\mathbf{Z}$. Here **dec8** works just like our routine **dec** above, and is checked in the same way. In brief **dec8**(x)=**8dec**($x/8$).

Our routine **subdivide** starts with a polygon $P \subset \mathbf{R}^4$ and adds one new point **interpolate**(v_i, v_{i+1}) between consecutive vertices v_i and v_{i+1} of P . This, the new polygon has twice as many vertices as the old one. Our routine **getPolygon** subdivides a polygon in \mathbf{R}^4 ten times and then projects it into T_8^4 using **dec8** componentwise on all the vertices.

We use a routine **getTracePoint** to get an interior point of Q . This routine returns the point **interpolate**($x_3, \text{interpolate}(x_1, x_2)$) where x_1, x_2, x_3 are the first three vertices of Q .

For each of the relevant indices (a_1, a_3, a_4, a_5) we let P be the polygon produced by **getPolygon** and we let $x \in P$ be the point produced by **getTracePoint**. Our next routine traces out the itinerary for x and returns a length 8 binary sequence. See §6.5. Recall that $C_k(\epsilon_k)$ for $\epsilon_k = \{0, 1\}$ are the two components on which the map \tilde{E}_k is defined.

getItinerary(x):

Let $x_1 = x$.

loop from $k = 1$ to 8.

Let $\epsilon_k \in \{0, 1\}$ be such that $x_k \in C_k(\epsilon_k)$.

Let $x_{k+1} = \tilde{E}_k(x_k)$.

return $\epsilon = \epsilon_1, \dots, \epsilon_8$.

Finally, for each vertex y of P we perform the following routine

verifyItinerary(ϵ, y):

Let $y_1 = y$. loop from $k = 1$ to 8.

Verify that $y_k \in C_k(\epsilon_k)$.

If false then return(**false**). Otherwise continue.

Let $y_{k+1} = \tilde{E}_k(y_k)$ using the ϵ_k extension of \tilde{E}_k .

return(**true**)

8 Appendix

8.1 The Polygons in the Partition

Here we list out the coordinates of the polygons in our partition \mathcal{P} of the torus Ω . These polygons are drawn in Figure 2.5. Each vertex of P_j has the form

$$\left(\frac{a_0 + a_1\phi}{2}, \frac{a_2 + a_3\phi}{2} \right).$$

We will simply list such a vertex as a row

$$a_0 \quad a_1 \quad a_2 \quad a_3$$

in an array whose other rows correspond to the other vertices of P_j .

$P1$ 5 -3 0 0 10 -6 -6 4 2 -1 0 0	$P2$ -5 3 0 0 -10 6 6 -4 -2 1 0 0	$P3$ 0 0 0 0 5 -3 0 0 10 -6 -6 4 5 -3 -6 4	
$P4$ 0 0 0 0 -5 3 0 0 -10 6 6 -4 -5 3 6 -4	$P5$ 0 0 0 0 13 -8 -6 4 5 -3 -6 4	$P6$ 0 0 0 0 -13 8 6 -4 -5 3 6 -4	$P7$ 9 -5 -4 4 4 -2 2 0 1 0 2 0 14 -8 -4 4
$P8$ -9 5 4 -4 -4 2 -2 0 -1 0 -2 0 -14 8 4 -4	$P9$ 3 -2 -4 2 -5 3 2 -2 3 -2 -2 0 -2 1 -2 0 6 -4 -8 4	$P10$ -3 2 4 -2 5 -3 -2 2 -3 2 2 0 2 -1 2 0 -6 4 8 -4	$P11$ 0 0 0 0 5 -3 -4 2 -3 2 0 0
$P12$ 0 0 0 0 -5 3 4 -2 3 -2 0 0	$P13$ 10 -6 -6 4 5 -3 -6 4 -3 2 4 -2	$P14$ -10 6 6 -4 -5 3 6 -4 3 -2 -4 2	$P15$ 13 -8 -6 4 5 -3 -6 4 -3 2 4 -2 5 -3 -2 2
$P16$ -13 8 6 -4 -5 3 6 -4 3 -2 -4 2 -5 3 2 -2	$P17$ 12 -8 -8 4 7 -5 -8 4 4 -3 -4 2	$P18$ -12 8 8 -4 -7 5 8 -4 -4 3 4 -2	$P19$ -4 2 -2 0 1 -1 -2 0 4 -3 -6 2
$P20$ 4 -2 2 0 -1 1 2 0 -4 3 6 -2	$P21$ 1 -1 0 0 6 -4 -6 4 -2 1 0 0	$P22$ -1 1 0 0 -6 4 6 -4 2 -1 0 0	$P23$ 6 -3 -2 2 -2 2 2 0 -4 3 4 -2 4 -2 0 0
$P24$ 1 -1 0 0 -2 1 0 0 3 -2 -4 2 1 -1 -2 0 -1 0 -2 0 4 -3 -4 2	$P25$ -1 1 0 0 2 -1 0 0 -3 2 4 -2 -1 1 2 0 1 0 2 0 -4 3 4 -2	$P26$ 0 0 0 0 5 -3 -4 2 0 0 -2 0 -5 3 2 -2	

8.2 The Dynamical Polygons

Here we list the 75 dynamical polygons associatd to the 75 genes. We use the same notation as above.

P_0 13 -8 0 0 -21 13 16 -10 13 -8 -10 6 5 -3 0 0	P_1 -15 9 8 -6 19 -12 -8 4 11 -7 -8 4 19 -12 -18 10	P_2 9 -5 -6 4 17 -10 -6 4 -17 11 10 -6 17 -10 -16 10	P_3 13 -8 -6 4 5 -3 -6 4 13 -8 -16 10 -21 13 10 -6
P_4 16 -10 -8 4 3 -2 -2 0 -10 6 -2 0 24 -15 -18 10	P_5 14 -8 -4 4 1 0 2 0 -12 8 2 0 22 -13 -14 10	P_6 19 -11 -8 6 -15 10 18 -10 -7 5 8 -4 -15 10 8 -4	P_7 10 -6 -6 4 5 -3 -6 4 -3 2 4 -2
P_8 -10 6 12 -8 3 -2 -4 2 16 -10 -14 8 24 -15 -14 8	P_9 -20 13 14 -8 1 0 -2 2 -12 8 14 -8	P_{10} -18 11 6 -4 3 -2 -10 6 -10 6 6 -4	P_{11} 23 -14 -16 10 10 -6 0 0 2 -1 0 0
P_{12} -16 10 14 -8 5 -3 -2 2 26 -16 -12 8 5 -3 -12 8	P_{13} -17 10 4 -4 -4 2 4 -4 17 -11 -12 6	P_{14} -12 8 14 -8 -20 13 14 -8 14 -8 -12 8 22 -13 -12 8	P_{15} -15 10 18 -10 19 -11 -8 6 -2 2 2 0
P_{16} -23 14 16 -10 -10 6 0 0 11 -7 -10 6	P_{17} 16 -10 -14 8 -5 3 2 -2 -26 16 12 -8 -5 3 12 -8	P_{18} 17 -10 -4 4 4 -2 -4 4 -4 3 6 -2	P_{19} 13 -8 0 0 -8 5 10 -6 0 0 0 0
P_{20} 24 -15 -18 10 3 -2 -8 4 16 -10 -8 4	P_{21} 1 0 -4 4 22 -13 -14 10 14 -8 -4 4	P_{22} -19 12 8 -4 -6 4 8 -4 2 -1 -2 2	P_{23} 9 -5 -2 2 -12 8 14 -8 -4 3 4 -2
P_{24} -5 3 4 -2 16 -10 -6 4 -5 3 -6 4 -26 16 20 -12	P_{25} 19 -12 -16 10 6 -4 0 0 -15 9 10 -6	P_{26} 17 -10 -16 10 -17 11 10 -6 4 -2 0 0	P_{27} 13 -8 -16 10 -21 13 10 -6 0 0 0 0
P_{28} 13 -8 0 0 -21 13 16 -10 0 0 0 0	P_{29} 19 -12 -8 4 6 -4 -8 4 -15 9 8 -6	P_{30} -9 5 2 -2 12 -8 -14 8 4 -3 -4 2	P_{31} 5 -3 -4 2 -16 10 6 -4 5 -3 6 -4 26 -16 -20 12
P_{32} -6 4 0 0 -19 12 16 -10 2 -1 0 0	P_{33} 4 -3 -2 0 -17 10 14 -10 -4 2 -2 0	P_{34} 24 -15 -14 8 16 -10 -14 8 3 -2 2 -2	P_{35} 14 -8 -12 8 22 -13 -12 8 1 0 4 -2
P_{36} -17 10 4 -4 -4 2 4 -4 4 -3 -6 2	P_{37} -13 8 0 0 8 -5 -10 6 0 0 0 0	P_{38} -16 10 8 -4 -3 2 2 0 10 -6 2 0 -24 15 18 -10	P_{39} -14 8 4 -4 -1 0 -2 0 12 -8 -2 0 -22 13 14 -10
P_{40} -10 6 6 -4 -5 3 6 -4 3 -2 -4 2	P_{41} -24 15 14 -8 -11 7 14 -8 10 -6 -12 8	P_{42} 26 -16 -20 12 5 -3 6 -4 -8 5 6 -4	P_{43} -19 12 16 -10 -6 4 0 0 15 -9 -10 6

<i>P44</i>	<i>P45</i>	<i>P46</i>	<i>P47</i>
-13 8 16 -10 21 -13 -10 6 0 0 0 0	-24 15 18 -10 -3 2 8 -4 -16 10 8 -4	-1 0 4 -4 -22 13 14 -10 -14 8 4 -4	19 -12 -8 4 6 -4 -8 4 -2 1 2 -2
<i>P48</i>	<i>P49</i>	<i>P50</i>	<i>P51</i>
18 -11 -10 6 5 -3 6 -4 -16 10 6 -4	-10 6 -2 0 24 -15 -18 10 11 -7 -2 0	-12 8 2 0 22 -13 -14 10 9 -5 2 0	24 -15 -14 8 11 -7 -14 8 -10 6 12 -8
<i>P52</i>	<i>P53</i>	<i>P54</i>	<i>P55</i>
9 -5 -12 8 22 -13 -12 8 -12 8 14 -8	-26 16 20 -12 -5 3 -6 4 8 -5 -6 4	6 -4 0 0 19 -12 -16 10 -2 1 0 0	-4 3 2 0 17 -10 -14 10 4 -2 2 0
<i>P56</i>	<i>P57</i>	<i>P58</i>	<i>P59</i>
-24 15 14 -8 -16 10 14 -8 -3 2 -2 2	-13 8 0 0 21 -13 -16 10 0 0 0 0	-19 12 8 -4 -6 4 8 -4 15 -9 -8 6	-18 11 10 -6 -5 3 -6 4 16 -10 -6 4
<i>P60</i>	<i>P61</i>	<i>P62</i>	<i>P63</i>
10 -6 2 0 -24 15 18 -10 -11 7 2 0	12 -8 -2 0 -22 13 14 -10 -9 5 -2 0	10 -6 -12 8 -3 2 4 -2 -16 10 14 -8 -24 15 14 -8	18 -11 -6 4 -3 2 10 -6 10 -6 -6 4
<i>P64</i>	<i>P65</i>	<i>P66</i>	<i>P67</i>
-23 14 16 -10 -10 6 0 0 -2 1 0 0	-13 8 0 0 21 -13 -16 10 -13 8 10 -6 -5 3 0 0	15 -9 -8 6 -19 12 8 -4 -11 7 8 -4 -19 12 18 -10	-13 8 6 -4 -5 3 6 -4 -13 8 16 -10 21 -13 -10 6
<i>P68</i>	<i>P69</i>	<i>P70</i>	<i>P71</i>
-26 16 12 -8 -5 3 12 -8 8 -5 -4 2	17 -10 -4 4 4 -2 -4 4 -17 11 12 -6	-5 3 12 -8 -18 11 12 -8 16 -10 -14 8	14 -8 -12 8 -20 13 14 -8 -7 5 14 -8
	<i>P72</i>	<i>P73</i>	<i>P74</i>
	26 -16 -12 8 5 -3 -12 8 -8 5 4 -2	23 -14 -16 10 10 -6 0 0 -11 7 10 -6	5 -3 -12 8 18 -11 -12 8 -16 10 14 -8

8.3 The Gene Locations

Here we list the coordinates for the points a_0, \dots, a_{74} . The point a_j is the central vertex of the gene A_j .

$a0$	$a1$	$a2$	$a3$	$a4$	$a5$	$a6$	$a7$	$a8$	$a9$
3	4	4	4	4	4	3	5	6	6
4	5	6	7	10	11	13	15	16	17
$a10$	$a11$	$a12$	$a13$	$a14$	$a15$	$a16$	$a17$	$a18$	$a19$
7	8	10	11	14	16	16	14	13	12
19	16	17	16	20	31	33	32	33	31

a_{20}	a_{21}	a_{22}	a_{23}	a_{24}	a_{15}	a_{26}	a_{27}	a_{28}	a_{29}
17	17	15	14	13	12	12	12	16	17
49	50	50	49	50	50	51	52	64	65
a_{30}	a_{31}	a_{32}	a_{33}	a_{34}	a_{35}	a_{36}	a_{37}	a_{38}	a_{39}
18	19	20	20	22	22	32	33	33	33
66	65	65	64	64	65	79	81	78	77
a_{40}	a_{41}	a_{42}	a_{43}	a_{44}	a_{45}	a_{46}	a_{47}	a_{48}	a_{49}
32	31	32	41	41	41	41	43	45	46
73	72	70	73	71	68	67	67	67	68
a_{50}	a_{51}	a_{52}	a_{53}	a_{54}	a_{55}	a_{56}	a_{57}	a_{58}	a_{59}
46	69	69	68	67	67	65	63	62	55
69	137	138	139	139	140	140	137	136	142
a_{60}	a_{61}	a_{62}	a_{63}	a_{64}	a_{65}	a_{66}	a_{67}	a_{68}	a_{69}
54	54	52	51	50	63	62	62	61	55
141	140	135	132	135	213	212	210	207	214
		a_{70}	a_{71}	a_{72}	a_{73}	a_{74}			
		48	48	73	76	86			
		210	211	282	275	279			

8.4 The Inflation Data

Here we list the date for the strands A'_0, \dots, A'_{74} that are associated to the genes A_0, \dots, A_{74} . The listing

A_j
 x_0
 y_0
 x_1
 y_1
 x_2
 y_2

68

indicates that the two endpoints of A_j are (x_0, y_0) and (x_2, y_2) , and the point (x_1, y_1) is the one lying within 3 units from the center point of $D(A_j)$. (There might be several such points, but we make some choice in each case.) Here is the listing.

A_0	A_1	A_2	A_3	A_4	A_5	A_6	A_7	A_8	A_9	A_{10}	A_{11}	A_{12}
9	11	15	17	12	15	12	15	21	25	24	33	37
17	16	22	25	39	43	50	64	63	68	76	73	72
11	16	17	16	16	17	12	21	25	24	31	34	41
17	22	25	30	43	46	56	63	69	72	80	68	72
15	17	16	12	17	12	12	25	24	24	34	37	41
22	25	30	34	46	50	60	68	71	76	76	72	67
A_{13}	A_{14}	A_{15}	A_{16}	A_{17}	A_{18}	A_{19}	A_{20}	A_{21}	A_{22}	A_{23}	A_{24}	A_{25}
41	59	67	67	62	58	54	67	71	66	63	58	51
67	81	128	136	136	140	136	204	208	217	208	212	208
46	58	67	67	59	54	51	71	71	62	58	54	50
69	85	132	140	137	140	132	208	213	211	208	212	211
45	58	67	62	58	54	46	71	66	63	58	51	51
71	89	136	135	140	136	136	212	217	208	212	208	216
A_{26}	A_{27}	A_{28}	A_{29}	A_{30}	A_{31}	A_{32}	A_{33}	A_{34}	A_{35}	A_{36}	A_{37}	A_{38}
52	51	64	67	72	78	85	85	89	92	130	134	143
211	216	271	272	279	275	279	276	267	271	334	338	335
51	50	68	71	75	79	84	86	92	92	135	138	139
216	221	272	276	280	276	276	270	271	276	336	344	331
50	46	71	72	76	84	84	89	92	92	134	143	139
221	225	276	279	275	279	271	267	275	280	338	340	326
A_{39}	A_{40}	A_{41}	A_{42}	A_{43}	A_{44}	A_{45}	A_{46}	A_{47}	A_{48}	A_{49}	A_{50}	A_{51}
140	140	135	132	174	173	177	172	178	187	189	193	288
331	310	309	297	313	305	293	288	280	284	283	289	576
141	135	130	134	173	175	172	175	181	189	194	195	291
325	310	305	297	310	300	287	283	284	284	289	292	580
143	130	130	139	173	177	173	178	181	193	195	190	291
322	305	301	300	305	297	284	280	288	289	292	296	584
A_{52}	A_{53}	A_{54}	A_{55}	A_{56}	A_{57}	A_{58}	A_{59}	A_{60}	A_{61}	A_{62}	A_{63}	A_{64}
291	291	284	285	279	271	266	237	232	229	224	219	211
580	589	585	588	597	580	581	600	602	598	576	563	568
291	287	283	284	274	265	261	231	228	230	219	216	211
585	589	588	593	593	581	575	602	598	592	572	559	572
291	284	284	279	274	261	262	228	228	232	219	211	206
589	585	593	597	589	575	572	598	593	589	568	563	567
A_{65}	A_{66}	A_{67}	A_{68}	A_{69}	A_{70}	A_{71}	A_{72}	A_{73}	A_{74}			
271	266	262	261	236	206	203	303	321	359			
902	903	894	877	907	890	890	1195	1170	1182			
265	261	264	258	233	203	202	308	322	363			
903	897	889	878	906	891	894	1195	1165	1182			
261	262	267	257	231	202	202	308	325	363			
897	894	885	881	903	894	898	1190	1169	1177			

9 References

- [D], R. Douady, *These de 3-eme cycle*, Universite de Paris 7, 1982
- [DT] F. Dogru and S. Tabachnikov, *Dual Billiards*, Math Intelligencer vo. 27 No. 4 (2005) 18–25
- [G] D. Genin, *Regular and Chaotic Dynamics of Outer Billiards*, Penn State Ph.D. thesis (2005)
- [GS] E. Gutkin and N. Simanyi, *Dual polygonal billiard and necklace dynamics*, Comm. Math. Phys. **143** (1991) 431–450
- [Ke] R. Kenyon, *Inflationary tilings with a similarity structure*, Comment. Math. Helv. **69** (1994) 169–198
- [Ko] Kolodziej, *The antibilliard outside a polygon*, Bull. Polish Acad Sci. Math. **37** (1989) 163–168
- [M] J. Moser, *Stable and Random Motions in Dynamical Systems, with Special Emphasis on Celestial Mechanics*, Annals of Math Studies **77**, Princeton University Press (1973)
- [N] B.H. Neumann, *Sharing Ham and Eggs*, summary of a Manchester Mathematics Colloquium, 25 Jan 1959 published in Iota, the Manchester University Mathematics students’ journal
- [T] S. Tabachnikov, *Geometry and Billiards*, A.M.S. Mathematics Advanced Study Semesters (2005)
- [VS] F. Vivaldi, A. Shaidenko, *Global stability of a class of discontinuous dual billiards*, Comm. Math. Phys. **110** (1987) 625–640